Predicting the Energy of the Water Exchange Reaction and Free Energy of Solvation for the Uranyl Ion in Aqueous Solution

Keith E. Gutowski and David. A Dixon*

Department of Chemistry and Center for Green Manufacturing, Shelby Hall, Box 870336, The University of Alabama, Tuscaloosa, Alabama 35487

Received: March 24, 2006; In Final Form: May 11, 2006

The structures and vibrational frequencies of $UO_2(H_2O)_4^{2+}$ and $UO_2(H_2O)_5^{2+}$ have been calculated using density functional theory and are in reasonable agreement with experiment. The energies of various reactions were calculated at the density functional theory (DFT) and MP2 levels; the latter provides the best results. Self-consistent reaction field calculations in the PCM and SCIPCM approximations predicted the free energy of the water exchange reaction, $UO_2(H_2O)_4^{2+} + H_2O \leftrightarrow UO_2(H_2O)_5^{2+}$. The calculated free energies of reaction are very sensitive to the choice of radii (O and H) and isodensity values in the PCM and SCIPCM models, respectively. Results consistent with the experimental HEXS value of -1.19 ± 0.42 kcal/mol (within 1−3 kcal/mol) are obtained with small cavities. The structures and vibrational frequencies of the clusters with second solvation shell waters: $UO_2(H_2O)_4(H_2O)_8^{2+}$, $UO_2(H_2O)_4(H_2O)_{10}^{2+}$, $UO_2(H_2O)_4(H_2O)_{11}^{2+}$, $UO_2(H_2O)_5(H_2O)_7^{2+}$, and $UO_2(H_2O)_5(H_2O)_{10}^{2+}$, were calculated and are in better agreement with experiment as compared to reactions involving only $UO_2(H_2O)_4^{2+}$ and $UO_2(H_2O)_5^{2+}$. The MP2 reaction energies for water exchange gave gas-phase results that agreed with experiment in the range -5.5 to $+3.3$ kcal/mol. The results were improved by inclusion of a standard PCM model with differences of -1.2 to $+2.7$ kcal/mol. Rearrangement reactions based on an intramolecular isomerization leading to a redistribution of water in the two shells provide good values in comparison to experiment with values of $\Delta G_{exchange}$ from -2.2 to -0.5 kcal/mol so the inclusion of a second hydration sphere accounts for most solvation effects. Calculation of the free energy of solvation of the uranyl cation yielded an upper bound to the solvation energy of -410 ± 5 kcal/mol, consistent with the best experimental value of -421 ± 15 kcal/mol.

Introduction

The solution chemistry of the early actinide metal cations has been the subject of a variety of experimental studies focused on elucidating their speciation in aqueous systems.[1] There is a need to understand the behavior of this series of elements in solution, including the separation of actinide ions in aqueous waste streams and modeling their behavior in the subsurface, particularly with respect to cleaning up the United States Department of Energy nuclear weapons production facilities, for example, the Hanford site. The solution chemistry of the uranyl cation, UO_2^{2+} has been studied extensively due to its stability under oxic conditions. In addition, there are a large number of solid-state crystal structures of the uranyl cation, indicative of its ubiquitous nature.[2] The uranyl cation, a linear moiety with trans oxo ligands, typically exists in solution as a complex ion with ligands bound equatorially to the uranium center. In most cases, the uranyl cation acts as a Lewis acid by accepting lone-pair electrons from ligands in the equatorial plane, which act as Lewis bases. Instances of the uranyl cation acting as a Lewis base have also been documented but are quite rare due to the very low partial negative charges on the oxo ligands.[3] In the presence of strongly coordinating ligands such as OH^-, NO_3^-, and CO_3^{2-}, complexes with octahedral, pentagonal bipyrimidal, and hexagonal bipyramidal geometries result due to bonding of 4, 5, or 6 atoms, respectively, in the equatorial plane.[4] The total number of ligands varies depending on the chelation mode (monodentate or bidentate) and steric factors. Although U−O equatorial bonds are typically strong and routinely observed, the binding of ligands containing other donating atoms such as C, N or S, as well as halide atoms, is also possible.[2,5] Several studies have also indicated the importance of charge transfer in these types of ligand complexes from the ligand to the uranyl ion, as well as significant polarization of the ligands themselves.[6] Clavaguéra-Sarrio et al.[7] showed that explicit polarization and charge-transfer effects must be treated explicitly in deriving a model potential for uranyl-water binding.

In aqueous systems in the absence of strongly coordinating ligands, the diffuse charge nature of noncoordinating counterions results in little to no direct observable binding to the uranyl ion. Extended X-ray absorption fine structure (EXAFS) spectroscopy measurements have confirmed the noncoordinating nature of, for example, the perchlorate anion (ClO_4^-) to the uranyl cation over a range of ClO_4^- concentrations.[8] If there are no other ligands to bind to the metal ion, water molecules will coordinate to the metal to form the first coordination shell. The effective inner coordination shell around a metal ion can often be treated as being rigid for the purposes of interpreting spectral properties,[9] although the actual dynamics can and do lead to exchange of these inner shell water molecules with those in the bulk solvent.[10] The structure of water in outer solvation shells is characterized by dynamic movement and exchange of water molecules leading to a lack of a rigid defined structure. Experimental investigations of the nature of $UO_2(H_2O)_n^{2+}$ aquo

* Corresponding author. E-mail: dadixon@bama.ua.edu.

10.1021/jp061851h CCC: $33.50
Published on Web 06/23/2006

ions have been performed using a variety of techniques, including X-ray diffraction (both single-crystal and solution), Raman and IR spectroscopies, EXAFS, NMR, and high-energy X-ray scattering (HEXS). Raman and IR studies of the $UO_2(H_2O)_n^{2+}$ ion(s) provide information on the bond stretching of the UO_2^{2+} moiety in aqueous solution, with symmetric and asymmetric stretching frequencies of about 870 and 961 cm^{-1}, respectively.[11] X-ray diffraction studies of uranyl perchlorate solutions are consistent with a pentagonal bipyramidal geometry with U═O and $U-O_{eq}$ bond distances of 1.702(5) and 2.421(5) Å, respectively, although it is generally agreed that the reported U═O length is anomalously short.[12] Low temperature ^1H NMR measurements also show a coordination number of 5, and it was suggested that this is also true at room temperature.[12,13] Single-crystal X-ray crystallographic studies of $UO_2[ClO_4]_2 \cdot 7H_2O$,[14] $[UO_2(H_2O)_5](ClO_4)_2$,[15] $[UO_2(H_2O)_5](ClO_4)_2 \cdot 2H_2O$,[15] and $[UO_2(H_2O)_5](CF_3SO_3)_2 \cdot C_{12}H_{24}O_6$[16] show pentagonal bipyrimidal geometries in the solid state as well, with only water molecules bound equatorially to the uranyl ion at $U-O_{eq}$ lengths of 2.45, 2.42, 2.41 and 2.41 Å, respectively. Interestingly, the structure of $UO_2(ClO_4)_2(H_2O)_3$ contains two equatorially bound ClO_4^- ligands.[15] EXAFS has been used to elucidate details of the structural nature of these aquo ions in solution as the scattering of X-ray photoelectrons is dependent upon the number and type of nearest neighbors. EXAFS data fits have indicated a coordination number of $n = 5$ corresponding to the $UO_2(H_2O)_5^{2+}$ as the favored species in aqueous perchlorate solutions. The $U-O_{eq}$ bond distance was determined to be 2.41 Å for these water molecules,[8,17] consistent with the X-ray diffraction studies in solution and the solid state.

Although the majority of experimental measurements indicate that the $UO_2(H_2O)_5^{2+}$ is the dominant species in aqueous solutions (in the presence of noncoordinating ligands), there is experimental evidence suggesting that $UO_2(H_2O)_4^{2+}$ may also be a minor component of these systems. For example, both NMR and EXAFS studies have indicated coordination numbers below 5, although it is typically concluded that the value is likely 5 in solution. The interpretation of HEXS measurements[18] of the uranyl ion in perchlorate media recently showed that an equilibrium exists in solution between the four- and five-coordinate uranyl:

$$UO_2(H_2O)_4^{2+} + H_2O \rightleftharpoons UO_2(H_2O)_5^{2+} \qquad (1)$$

Integration of the HEXS peak at 2.420(1) Å yielded 46.1 electrons, 3.9 electrons short of the number that would correspond to five-coordinating water molecules. As it is chemically unlikely that nearly four electrons are transferred to the uranyl ion, it was concluded that an equilibrium between four- and five-coordinated water molecules accounts for this difference. Modeling of the data yielded an equilibrium with the five-coordinate uranyl favored over four-coordinate by 86(7)% to 14(7)%. This yielded the result that at the given experimental conditions, five-coordinate uranyl is more stable than the counterpart by -1.19 ± 0.42 kcal/mol at 298 K.

Quantum chemical studies of the uranyl ion in both the gas phase and solution phase can provide insight into properties that are difficult to measure experimentally. Until recently, computational studies of heavy elements, particularly actinides, were challenging because of the large number of electrons and the importance of relativistic effects. However, with the development of density functional methods and relativistic effective core potentials, the treatment of actinide-containing complexes has become more routine and the results more reliable.[19] In addition, calculations using modern computational techniques and continuum dielectric approaches[20] have been used to predict the solution structure and behavior of a range of metal cations, including alkali,[21] alkaline earth,[22] transition metal,[21−23] and lanthanide cations.[24] Pratt and co-workers have developed the quasi-chemical approach[25] to provide a more formal basis to the prediction of solvation free energies based on combining the binding energy of the cluster to an ion with a continuum dielectric model of the remaining solvent. The approach developed by us[26] for predicting the free energies of solvation for ions is essentially the same as the Pratt approach except that we have used a cluster of n water molecules as a reactant instead of n single water molecules to minimize differences in the nonelectrostatic parts of the long-range interaction with the continuum. With our reactant cluster approach, it would be difficult to change the pressure from the standard state.

Progress has also been made in using solvation approaches to describe water-exchange mechanisms in transition metals.[27] One of the earliest studies on the hydration of the UO_2^{2+} cation was performed by Spencer et al.[28] who performed DFT calculations with the BLYP exchange−correlation functional on $UO_2(H_2O)_n^{2+}$ ($n = 4-6$) complexes in both the gas and aqueous phases, using the Hay RECP and basis set[29] on uranium and a DZP basis set on H and O. Their solvation approach used a simple dielectric continuum approach with an ellipsoidal cavity and found that the five-coordinate is lower in energy than the four-coordinate complex by −7.2 kcal/mol. A previous study has shown that spherical and molecular-shaped cavities can produce opposing trends in metal−oxygen bond distances upon inclusion of solvation effects.[30] Spencer et al. concluded that the $n = 5$ structure was the most stable structure in both the gas and liquid phases, and that solvent effects are critical for predicting ligand-binding properties, although no predictions of relative free energies in solution were provided. They also noted significant amounts of charge transfer from the water to the uranyl so that the solvent water molecules are acting like actual binding equatorial ligands. Hay et al.[31] reported different results for the stability of the $n = 5$ structure in the gas phase versus aqueous solution. Using the B3LYP exchange−correlation functional with the Hay and Martin 78 e RECP and basis set[32] on uranium and 6-31G* basis set on H and O, they predicted that the $n = 6$ structure is the most stable in the gas phase, with the $n = 5$ structure becoming the most stable when solvation effects are included. They also reported a free energy of reaction in solution for reaction 1 of −6.5 kcal/mol, which differs from the experimental HEXS value by greater than 5 kcal/mol. We do note that these calculations were done before the experimental HEXS measurement. Tsushima and Suzuki[33] performed MP2 calculations (with the Ortiz et al. basis set and RECP[34] on uranium and the 6-311G** basis set on H and O) on uranyl aquo ions with $n = 3-5$, as well as QM/MM calculations on the second hydration sphere with 6−12 explicitly included water molecules. They predict the $n = 5$ structure to be the most stable and predicted structural parameters from the MP2 calculations in good agreement with experimental results. They noted that inclusion of the second hydration sphere was important for predicting the hydration number of the uranyl ion. Tsushima et al.[35] used a polarizable continuum model and the B3LYP functional with the Ortiz et al. basis set and RECP on uranium[34] and 6-31++G** on H and O to predict a hydration number for uranyl in the liquid phase of five. Fuchs et al.[36] calculated the free energy difference for reaction 1 with the COSMO approach at the all-electron scalar relativistic LCGTO−FF-DF level (Minami and Matsuoka basis set[37] on uranium and

standard Gaussian basis sets on H and O[38]) to be −7.3 kcal/mol. They also predict a solvation energy of −407 kcal/mol consistent with the experimental value of −402 ± 60 kcal/mol derived from an ICR measurement[39] but not with the earlier values near −320 kcal/mol.[40] Recent molecular dynamics simulations by Hagberg et al.[41] using a force field developed for the study of uranyl in aqueous solution support the presence of five-coordinated water molecules in the equatorial plane with no hydrogen bonding between the oxo ligands of uranyl and waters of the outer hydration spheres.

Bühl et al.[42] recently reported a Car−Parrinello molecular dynamics (CPMD) simulation of the water exchange reaction. Using the BLYP functional, their gas-phase CPMD simulation indicated that the four-coordinate structure with a hydrogen-bonded second sphere water is more stable than the five-coordinate one by 2.2 kcal/mol. In addition, a CPMD simulation in bulk water (total of 66 water molecules) suggests that the five-coordinate becomes more stable than the four-coordinate counterpart by 8.7 kcal/mol. Their use of the BLYP functional results in a gas-phase reaction energy for reaction 1 of −20.6 kcal/mol, which is higher (less negative) than many reported literature values.

More recent computational studies have focused on the free energy of hydration of the uranyl cation because of the considerable uncertainty in the experimental measurement. Moskaleva et al.[43] performed all electron calculations[37,38] using the LCGTO−FF-DF approach with the VWN (local) and BP functionals and COSMO solvation to examine the stability of various aquo ion species in solution, as well as evaluate the hydration free energy of the uranyl ion. With a DFT treatment of the first shell using the BP functional and a continuum treatment of the remaining solvent, they predict a solvation free energy for the uranyl ion of −422 kcal/mol, which is consistent with the value derived from the ICR data, although they suggest that this solvation energy could be too large and should be shifted to −372 to −382 kcal/mol. They predict that the five-coordinate and six-coordinate uranyl aquo ions are equally stable in solution, which disagrees with Hay et al.[31] and a variety of experimental measurements, including NMR, EXAFS, and HEXS, which indicate five-coordinate uranyl in aqueous solution. Cao and Balasubramanian[44] reported similar results with respect to the uranyl solvation energy and the equal preference of the five-coordinate and six-coordinate structure in solution using a PCM solvation model (with varying radii) with DFT/B3LYP, MP2, and CCSD calculations (78 e core on uranium from Ermler et al.,[45] RECP and basis set on O,[46] and van Duijneveldt's basis set on H[47]). They state that the solvation free energy of the uranyl ion is best treated in the method of Moskaleva et al. and the solvation energies varied in the range −405 to −435 kcal/mol at the B3LYP level and −432 to −472 kcal/mol at the MP2 level, depending on the atomic radii used in the PCM model. These values are again within the range of the predictions from the ICR data considering the large error bars of ±60 kcal/mol. Shamov and Schrechenbach[48] studied the solvation free energy of the uranyl ion using COSMO and CPCM solvation with the hybrid B3LYP and generalized gradient approximation (GGA) PBE functionals (the former with a 60 e RECP and basis set[49] for uranium and 6-31G* on H and O and the latter at the all-electron ZORA level). Using the pentaaquo ion as well as larger clusters with explicit water molecules in the second shell, they obtained a free energy of −384 kcal/mol for the former and between −407 and −425 kcal/mol for the latter clusters. The cluster results are in good agreement with an estimated value of −421 ± 15 kcal/mol that the authors refined from experimental data of Marcus[50] and Gibson et al.[51]

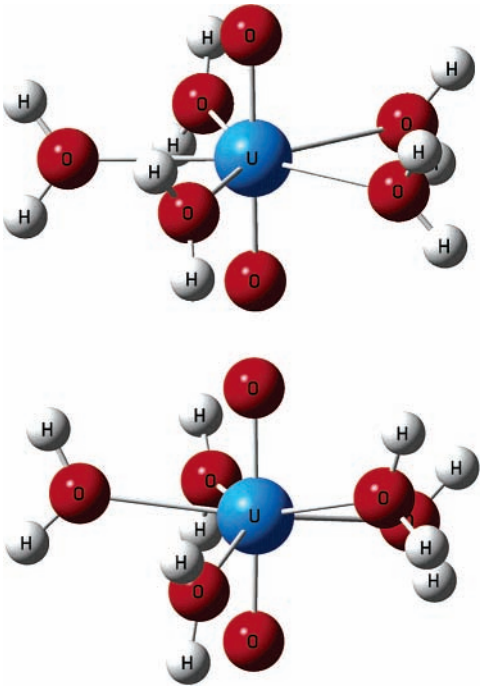

Figure 1. Gas-phase structures of $UO_2(H_2O)_5^{2+}$ at B3LYP (D_5, top) and SVWN (C_1, bottom) levels.

In the current study, we have used electronic structure calculations at the density functional theory (DFT) and molecular orbital (MO) theory levels on molecular clusters coupled with continuum solvation models to predict the free energy of reaction of reaction 1. First, gas-phase and solution-phase structural details of the $UO_2(H_2O)_4^{2+}$ and $UO_2(H_2O)_5^{2+}$ aquo ions are reported and compared with experimental and other theoretical literature values. Next, gas-phase values for the free energy of reaction for reaction 1 are reported at both the MP2 and DFT levels including the effects of basis set size on the light atoms as well as higher angular momentum functions on the uranium. A comprehensive study on solvation effects from self-consistent reaction field (SCRF) models is reported and the effects on cavity size are discussed. Optimized clusters that include part of the second solvation shell, $UO_2(H_2O)_4(H_2O)_8^{2+}$, $UO_2(H_2O)_4(H_2O)_{10}^{2+}$, $UO_2(H_2O)_4(H_2O)_{11}^{2+}$, $UO_2(H_2O)_5(H_2O)_7^{2+}$, and $UO_2(H_2O)_5(H_2O)_{10}^{2+}$, are used to evaluate the water exchange energetics in conjunction with including the effects of SCRF models. Finally, we estimate the free energy of solvation of uranyl in aqueous solution.

Computational Methods

The optimized structures of $UO_2(H_2O)_5^{2+}$ and $UO_2(H_2O)_4^{2+}$ with the gradient corrected hybrid B3LYP[52] and local SVWN[53] exchange−correlation functionals are shown in Figures 1 and 2. Previous studies on UO_2^{2+} have shown that good agreement as compared to the fully relativistic CCSD(T) calculations can be obtained with the small core Stuttgart RECP and associated Stuttgart orbital basis sets[54] for U and valence triple-ζ plus polarization (TZVP) DFT optimized basis sets[55] for the oxygen atoms. All of our DFT geometry optimizations and frequency calculations were done with the Stuttgart small core RECPs and the corresponding Stuttgart orbital basis sets for the U atom and the TZVP orbital basis set for the O and H atoms. In addition, DFT calculations with the aug-cc-pVnZ (n = D, T, Q)[56] on O and H were also performed for comparison purposes

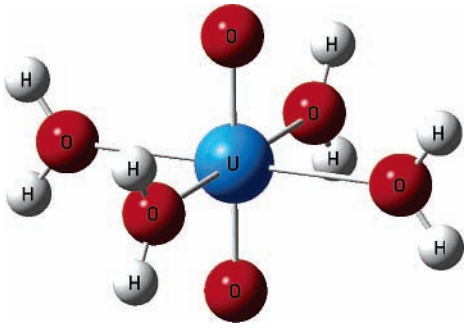

Figure 2. Gas-phase structure of $UO_2(H_2O)_4^{2+}$ at both the B3LYP and SVWN levels (D_{4h}).

and to examine the effect of basis set size. In all cases, spherical basis sets were employed. We eliminated the most diffuse functions in the U basis set, those with an exponent of 0.005. These were deleted due to the difficulty in converging the wave function with such diffuse functions, in part due to the types of grids that were used. These diffuse functions were replaced with less diffuse exponents of 0.013, 0.059, 0.026, and 0.067 for the s, p, d, and f functions, obtained by geometric extrapoloation.[57] Single-point MP2 calculations at the optimized DFT geometries were also performed on the uranyl aquo ions employing the modified Stuttgart small core basis set (with and without added g functions and corresponding ECP with the aug-cc-pVnZ (n = D, T, Q) basis sets on the light atoms. We did not find significant BSSE effects on expanding the size of the basis set, so for the larger clusters, the single-point MP2 calculations were done with the aug-cc-pVTZ basis sets on the light atoms and the modified Stuttgart RECP and basis set with g functions. MP2 calculations were performed with the 1s core orbitals frozen on oxygen atoms and 5s, 5p, and 5d orbitals frozen on uranium following other workers.[58] Thermochemical corrections to the MP2 energies to obtain the free energies were done using the geometries and frequencies obtained at the B3LYP/aug-cc-pVTZ level for the $UO_2(H_2O)_n^{2+}$ ions (up to $n = 5$) and at the B3LYP/TZVP level for the large clusters. All calculations were performed with the Gaussian03[59] suite of programs on the SGI Altix 350 and Cray XD1 at the Alabama Supercomputer Center and the NWChem suite of programs[60] on the massively parallel 1980 processor HP Linux cluster in the Molecular Science Computing Facility in the William R. Wiley Environmental Molecular Sciences laboratory at the Pacific Northwest National Laboratory.

Solvation effects were included through the use of the polarizable continuum model (PCM),[61] conductor-like polarizable continuum model (CPCM),[62] and self-consistent isodensity polarizable continuum model (SCIPCM)[63] as implemented in Gaussian03. A dielectric constant of 78.39 was used corresponding to that for water as the solvent. COSMO,[64] an implementation of the conductor-like polarizable continuum model employing Klamt radii, was also used. Cavity effects in the CPCM and PCM approaches were studied using the radii obtained by using the UA0[65a], UFF,[65a] UAHF,[65b] UAKS,[59] Pauling,[65c] and Bondi[65d] radii as implemented in Gaussian03. Klamt radii[64] were used in the PCM model to perform a COSMO calculation. The radii are given in Table 1. SCIPCM calculations were performed with different isodensity values, a 974 integration point Lebedev grid, and integration using a single origin. Natural bond orbital (NBO) analyses were performed at the optimized geometries at the B3LYP DFT level with the program Gaussian03.[66]

TABLE 1: Atom Radii (Å) for U, O, and H for Use in the PCM Model

cavity	U	O	H	O + H
UA0	1.698	1.750	-	1.950
UFF	1.698	1.750	1.443	
UAHF	1.698	1.590	-	1.680
UAKS	1.698	1.500	-	1.680
Klamt	2.00	1.72	1.30	-
Pauling	1.86	1.40	1.20	-
Bondi	1.86	1.52	1.20	-

TABLE 2: Relative Electronic Energies (kcal/mol) of $UO_2(H_2O)_5^{2+}$ Structures

structure	symm	rel energy	no. imag modes
B3LYP	D_{5h}	0.32	3
B3LYP	D_5	0.06	0
B3LYP	C_1	0.00	0
SVWN	D_5	0.79	2
SVWN	C_1	0.00	0

Results and Discussion

Gas-Phase Structure and Energetics. The optimized gas-phase structures of $UO_2(H_2O)_5^{2+}$ at the B3LYP and SVWN levels are shown in Figure 1. For each DFT functional, different symmetries were enforced, and the resulting relative energies between these structures are listed in Table 2. At the B3LYP level, structures with C_1, D_5, and D_{5h} symmetries were studied. The U═O and U−O_{eq} bond distances remained identical for each of these structures upon optimization and only the OUOH dihedral angles varied (to a small extent) dependent on the symmetry. The C_1 structure was the most stable of the three, but only by 0.06 kcal/mol over the D_5 structure. Both the C_1 and D_5 structures were minima on the potential energy surface as indicated by the absence of imaginary frequencies in the vibrational analysis. This difference could well be due to inaccuracies in the grid, but the difference is so small as to not be chemically important. The D_{5h} structure with three imaginary frequencies was 0.32 kcal/mol higher in energy as compared to the lowest energy C_1 structure. The U═O and U−O_{eq} bond distances in the D_{5h} structure were identical to those in the C_1 and D_5 structures. The potential energy surface for rotating the dihedral angles of the water molecules is thus quite flat as indicated by the closeness of the relative energetic ordering of the structures. The low energy difference between the D_5 and C_1 structures suggests that the observed structure at 298 K is likely to have D_5 symmetry. As a result, the D_5 structure for the $UO_2(H_2O)_5^{2+}$ aquo ion was used throughout to take advantage of molecular symmetry in the calculations. In all structures, the U═O and U−O_{eq} bond lengths optimized to 1.75 and 2.50 Å, respectively, with a O═U═O angle of 180°. The symmetric and asymmetric stretching frequencies for the uranyl are 955 and 1043 cm^{-1} in the D_5 structure and show little variation for the three structures.

Previously we have shown that the geometries of the structures arising from the interaction of UO_2^{2+} with anions can be reliably predicted at the LDA level.[19b] However, these structures do not involve hydrogen bonds, which are potentially present in the uranyl−water clusters and involve a stronger Coulombic interaction than present in the water complexes. DFT with local exchange−correlation functionals leads to overbinding, especially of systems with important nonbonded interactions which are weakly bound.[67] The SVWN structure (Figure 1) was distinctly different from the B3LYP structure, having a distorted C_1 structure, with the D_5 structure lying 0.79 kcal/mol higher in energy (Table 2). Use of the SVWN functional resulted in U−O_{eq} bonds in the C_1 structure that were too short (2.406 Å),

TABLE 3: Calculated Geometric Gas-Phase Parameters Compared to Experimental Values in the Condensed State

structure	method	R(U═O), Å	R(U−$O_{eq.}$), Å	R(U−O_{second}),[a] Å	∠(O═U═O), deg
UO_2^{2+}	B3LYP	1.701			180.0
UO_2^{2+}	SVWN	1.703			180.0
$UO_2(H_2O)_4^{2+}$	B3LYP (D_{4h})	1.746	2.436		180.0
$UO_2(H_2O)_4^{2+}$	SVWN (D_{4h})	1.755	2.355		180.0
$UO_2(H_2O)_5^{2+}$	B3LYP (D_{5h})	1.748	2.500		180.0
$UO_2(H_2O)_5^{2+}$	B3LYP (D_5)	1.748	2.500		180.0
$UO_2(H_2O)_5^{2+}$	B3LYP (C_1)	1.748	2.500		180.0
$UO_2(H_2O)_5^{2+}$	SVWN (D_5)	1.758	2.413		180.0
$UO_2(H_2O)_5^{2+}$	SVWN (C_1)	1.761	2.406 (avg)		174.3
$UO_2(H_2O)_4(H_2O)_8^{2+}$	B3LYP (C_1)	1.765(0)	2.369(1)	4.48(1)[j]	180.0
$UO_2(H_2O)_4(H_2O)_{10}^{2+}$	B3LYP (C_1)	1.769(4)	2.363(29)	4.43(15)[j]	179.7
$UO_2(H_2O)_4(H_2O)_{11}^{2+}$	B3LYP (C_1)	1.770(2)	2.361(25)	4.45(9)[j]	179.2
$UO_2(H_2O)_5(H_2O)_7^{2+}$	B3LYP (C_1)	1.763(0)	2.442(1),[i] 2.546	4.45(16)[j]	178.1
$UO_2(H_2O)_5(H_2O)_{10}^{2+}$	B3LYP (C_1)	1.767(1)	2.433(5),[i] 2.525	4.64(19)[j]	177.3
HEXS[b]		1.766(1)	2.420(1)	4.50	
EXAFS		1.76(1),[g] 1.783(5)[h]	2.41(1),[g] 2.413(5)[h]		
XRD_{soln}[c]		1.702(5)	2.421(5)	4.37	
XRD_{solid}[d]		1.71(8)	2.45(10)		161(3)
XRD_{solid}[e]		1.76(2)	2.42(5)		177.3(9)
XRD_{solid}[e]		1.76(1)	2.41(1)		179.2(3)
XRD_{solid}[f]		1.76(1)	2.41(3)		179.0(1)

[a] Average of oxygen distances (with standard deviation) from second sphere waters involved in hydrogen bonding to primary sphere waters. [b] Reference 18. [c] Reference 12. [d] $UO_2[ClO_4]_2 \cdot 7H_2O$ (ref 14). [e] $[UO_2(H_2O)_5](ClO_4)_2$ (ref 15). [e] $[UO_2(H_2O)_5](ClO_4)_2 \cdot 2H_2O$ (ref 15). [f] $[UO_2(H_2O)_5](CF_3SO_3)_2 \cdot C_{12}H_{24}O_6$ (ref 16). [g] Reference 8a. [h] Reference 8b. [i] Average of the four short equatorial bonds. [j] (max, min) = (4.50, 4.47); (4.60, 4.23); (4.60, 4.34); (4.61, 4.16); (4.96, 4.35).

TABLE 4: Calculated Symmetric and Asymmetric UO_2^{2+} Stretching Frequencies (cm^{-1}) Compared to Experimental Values in the Condensed State

structure	method	ν_{sym}	ν_{asym}
UO_2^{2+}	B3LYP	1041.2	1140.7
UO_2^{2+}	SVWN	1018.8	1122.4
$UO_2(H_2O)_4^{2+}$	B3LYP (D_{4h})	961.9	1050.6
$UO_2(H_2O)_4^{2+}$	SVWN (D_{4h})	934.8	1026.1
$UO_2(H_2O)_5^{2+}$	B3LYP (D_{5h})	955.9	1044.4
$UO_2(H_2O)_5^{2+}$	B3LYP (D_5)	955.2	1043.4
$UO_2(H_2O)_5^{2+}$	B3LYP (C_1)	955.1	1043.4
$UO_2(H_2O)_5^{2+}$	SVWN (D_5)	926.8	1018.4
$UO_2(H_2O)_5^{2+}$	SVWN (C_1)	915.8	1008.7
$UO_2(H_2O)_4(H_2O)_8^{2+}$		921.3	1014.1
$UO_2(H_2O)_4(H_2O)_{10}^{2+}$		913.6	1007.7
$UO_2(H_2O)_4(H_2O)_{11}^{2+}$		910.3	1001.3
$UO_2(H_2O)_5(H_2O)_7^{2+}$		915.2, 927.6	1011.6
$UO_2(H_2O)_5(H_2O)_{10}^{2+}$		914.9	1009.6
Raman		869,[a] 870[b]	
IR			965,[c] 961[d]

[a] Reference 11a. [b] Reference 11b. [c] Reference 11c. [d] Reference 11d.

leading to repulsions between the neighboring oxygen atoms and significant deviation of the water molecules out of the equatorial plane. The U═O bond length (1.76 Å) was consistent with the B3LYP structure, but the O═U═O bond angle deviated from linearity at 174.3° due to the asymmetry of the structure and the low O═U═O bending mode of the isolated ion (∼150 cm^{-1}). The symmetric and asymmetric uranyl stretches occurred at 916 and 1009 cm^{-1}, respectively.

The predicted geometric and vibrational parameters in the gas phase are compared to available experimentally determined values in the condensed state in Tables 3 and 4. In the B3LYP D_5 structure, the U═O bond length is predicted to be too short by 0.012−0.035 Å as compared to the HEXS and EXAFS results (as well as the upper end of the solid-state XRD values). Additionally, the calculated U−O_{eq} bond lengths are too long by about 0.08−0.09 Å. This is consistent with the fact that the calculated values correspond to isolated ions in the gas phase as well as to the fact that the gradient corrected bond distances tend to be somewhat longer than the experimental values. In the condensed phase, the U═O bond should lengthen and the U−O_{eq} bonds should shorten on the basis of solvation effects. The predicted symmetric and asymmetric uranyl stretches are too high by 86 and 81 cm^{-1}, respectively, consistent with U═O bond distances that are too short. Although the geometry parameters for the SVWN structure were in good agreement with experiment (except for the O═U═O angle), this method is not appropriate for treating a second solvation shell so the B3LYP structure was used for our solvation predictions.

The optimized gas-phase structure of $UO_2(H_2O)_4^{2+}$ is illustrated in Figure 2. At both the B3LYP and SVWN levels, the D_{4h} structure is the most stable. This is consistent with previous reports in the literature and is due to less steric crowding in the equatorial region of the uranyl ion. The U═O distances at both the B3LYP and SVWN levels are 1.75 and 1.76 Å, but the U−O_{eq} distances (2.44 and 2.36 Å, respectively) differ slightly. This is consistent with the equatorial bond length shortening that occurred in the pentaaquo species at the SVWN level. The symmetric stretching frequencies for the uranyl are predicted to be at 962 and 935 cm^{-1} in the B3LYP and SVWN structures, respectively, and the asymmetric stretches are at 1051 and 1026 cm^{-1}. Considerable difficulty was encountered in obtaining an optimized gas-phase structure for $UO_2(H_2O)_6^{2+}$ with six atoms in the inner solvation shell due to the high degree of steric crowding in the equatorial region. Experimental results strongly suggest that six-coordinate uranyl aquo ions are not present to a large extent in solution, and therefore this species was not included in our analysis. Our result is also consistent with the results of Cao et al.[44] who find a structure with six water molecules in the gas phase to have five molecules in the inner shell with one water hydrogen bonded externally to this shell. This structure was predicted to be 5.3 kcal/mol more stable than a structure with six water molecules in the first solvation shell.[44]

The gas-phase energies, enthalpies, and free energies for reaction 1 at various levels of theory are provided in Table 5. The first five entries compare the gas-phase free energies obtained at the local and nonlocal DFT levels. The SVWN value differs significantly from the B3LYP values and this is due to

TABLE 5: Gas-Phase Energies, Enthalpies, and Free Energies (kcal/mol) at the DFT (B3LYP and SVWN) and MP2[a] Levels for Reaction 1

level	ΔE_{elec}	ΔZPE	ΔE_0	ΔE_{298}	ΔH_{298}	ΔG_{298}
B3LYP/TZVP	−24.5	1.0	−23.5	−22.6	−23.2	−15.8
B3LYP/aug-cc-pVDZ	−22.7	0.8	−21.9	−21.0	−21.6	−14.2
B3LYP/aug-cc-pVTZ	−22.9	1.2	−21.7	−21.0	−21.6	−13.5
B3LYP/aug-cc-pVQZ	−22.8	1.2	−21.5	−20.9	−21.5	−13.3
SVWN/TZVP	−33.3	1.8	−31.5	−31.2	−31.8	−24.3
MP2/aug-cc-pVDZ	−28.0	1.2	−26.8	−26.0	−26.6	−18.5
MP2/aug-cc-pVTZ	−27.8	1.2	−26.6	−25.9	−26.5	−18.4
MP2/aug-cc-pVQZ	−27.2	1.2	−26.0	−25.3	−25.9	−17.8
MP2/aug-cc-pVDZ (g)[b]	−27.3	1.2	−26.1	−25.3	−25.9	−17.8
MP2/aug-cc-pVTZ (g)[b]	−27.1	1.2	−25.9	−25.2	−25.8	−17.6
MP2/aug-cc-pVQZ (g)[b]	−26.9	1.2	−25.7	−25.0	−25.6	−17.5
DFT/B3LYP[c]	−28.9	1.7	−27.2			−19.3

[a] With B3LYP/aug-cc-pVTZ thermochemistry corrections. [b] (g) = added g functions on uranium basis set. [c] Reference 31.

the tendency of the local functional to overestimate ligand binding energies. For this reason, the SVWN energetics will not be discussed further. The value obtained at the B3LYP level, with the 6-31G* basis sets for O and H, and a large core (78 e) RECP and basis set on U are in significant disagreement with our best DFT calculations by nearly 6 kcal/mol.[31] It has been shown that the 78 e large core RECP of Hay and Martin[32] can result in a bent structure with a O═U═O angle of 153° at the DFT level.[68]

We also performed MP2 calculations with large basis sets to approach the complete basis set limit with up to aug-cc-pVQZ on the O and H atoms and including g functions on the small core Stuttgart uranium basis set. Inclusion of the g functions on the uranium basis set and using the largest aug-cc-pVQZ basis on O and H results in an increase in the reaction free energy of 1.0 kcal/mol over the no-g/aug-cc-pVDZ treatment, from −18.5 to −17.5 kcal/mol, consistent with the presence of some BSSE in the smaller basis set calculations. Our best MP2 free energy (−17.5 kca/mol) differs from our B3LYP/TZVP and B3LYP/aug-cc-pVQZ free energies by 1.7 and 4.2 kcal/mol, respectively, indicating that the B3LYP approach is somewhat overstabilizing the reactants in reaction 1 with respect to the MP2 approach. We have used the best MP2 gas-phase free energy as the baseline for later solvation corrections. This system should be well described by a single reference method, thus making use of MP2 appropriate. Single-point CCSD calculations of $UO_2(H_2O)_4^{2+}$ and $UO_2(H_2O)_5^{2+}$ with the U ECP and basis set and the aug-cc-pVDZ on O and H were performed to obtain the T_1 diagnostic to provide an estimate of the multireference character of these ions.[69] The T_1 diagnostics were 0.023 and 0.022, respectively, showing that a single reference wave function does provide an appropriate description of these systems.

Natural bond order (NBO) calculations were also performed to examine the importance of charge transfer in the $UO_2(H_2O)_n^{2+}$ aquo ions. Previous studies have commented on the significant amount of charge transfer that occurs, making the water molecules appear as actual equatorially bound ligands. Charge transfer was quantified as the group charge on the central uranyl moiety and was determined from B3LYP calculations. In the $UO_2(H_2O)_4^{2+}$ aquo ion, the NBO calculations show that 0.48 e was transferred to the uranyl, lowering the positive charge on the uranyl to +1.52 e. In the $UO_2(H_2O)_5^{2+}$, 0.52 e was transferred to the uranyl, slightly greater than in the tetraaquo ion, lowering the uranyl positive charge to +1.48 e.

Solution Thermodynamics. The general approach of using a continuum solvation model is the most computationally tractable method currently available, yet as shown below and consistent with other studies,[44,70] is very sensitive to the choice of parameters, especially if no waters of solvation are present. However, as shown in a number of studies on monatomic cations, the inclusion of explicit water molecules in the first hydration sphere is necessary to converge to reliable values of the free energy of solvation.[26] Inclusion of the second or higher order hydration spheres is generally not used due to the large size of the necessary clusters and the nonstatic nature of the second shell. As shown below, inclusion of more than the inner hydration shell does improve the results for the free energy of reaction for water exchange and does provide useful insights into the solution chemistry. Ab initio molecular dynamics simulations are also an alternative solution but are computationally intensive whereas MD methods based on classical force fields need to be carefully parametrized.[41]

The continuum-based solvation models used in this study partition the solute−solvent environment into two distinct regimes, one of which is a cavity containing the solute molecule, and the other is the solvent medium surrounding the cavity defined solely by its dielectric constant. Induced charges on the surface of the cavity due to solute−solvent polarization allow one to obtain the free energy of solution of the solute under study.[20] Table 6 contains the electrostatic and nonelectrostatic solution energy contributions to the free energy of reaction from the PCM, CPCM, and SCIPCM models as a function of atom radii (or isodensity value) (Table 1) and level of theory (B3LYP and SVWN) for the reaction defined in reaction 1. Examination of the data reveals that the solution energy contributions from the PCM and CPCM models are invariant with respect to the type of functional used. The maximum difference in the electrostatic contribution to the reaction free energy between the two methods is 2.6 kcal/mol with the CPCM (Pauling radii), and the overall average difference is 1.2 kcal/mol. The maximum difference in the nonelectrostatic contribution between the two methods is 0.8 kcal/mol, and the overall average difference is 0.5 kcal/mol. On the basis of the discussion of the dependence of the energetics and geometries on the functional, only the B3LYP values were used in the analysis of the final solution free energies. The comparable results for the B3LYP and SVWN functionals also show that the PCM and CPCM methods are relatively insensitive to the geometries of the uranyl aquo ions, as the optimized gas-phase structures for each methods are significantly different.

The PCM and CPCM approaches performed similarly as a function of the radii set. Within the B3LYP results, the difference in the electrostatic terms for the reaction free energy between PCM and CPCM was from 0.1 to 0.2 kcal/mol. This suggests that modifying the boundary problem by changing the dielectric value from a specific finite value to $\epsilon = \infty$ will introduce little change and thus both are equally well suited for studying the solution chemistry of the uranyl ion.

The nonelectrostatic contributions to the solution free energy for reaction 1, although accounting for only a small portion of the total energy contribution to the free energy of reaction in most cases (8.7% average for B3LYP/PCM), were included for completeness. It should be noted that in calculating the cavitation, dispersion, and repulsion contributions to the nonelectrostatic energy, the dispersion and repulsion contributions from uranium were neglected as no parameters are currently available.

The B3LYP results in Table 6 are most readily evaluated by comparing the atomic radii used to define the solute cavity, as well as the resultant cavity volumes and surface areas generated

TABLE 6: PCM, CPCM, and SCIPCM Solvation Energy Contributions (Electrostatic and Nonelectrostatic) (kcal/mol) for the Energy of Reaction 1[a]

		B3LYP			SVWN		
model	cavity parameter	electrostatic	nonelectrostatic	sum	electrostatic	nonelectrostatic	sum
PCM	UA0	13.4	−2.7	10.7	14.6	−2.8	11.8
	UFF	14.6	−1.3	13.3	14.6	−1.8	12.8
	UAKS	20.7	−0.7	20.0			
	UAKS (scaled)[b]	12.7	−0.7	12.0	13.9	−1.4	12.5
	UAHF	20.8	−0.8	20.0			
	UAHF (scaled)[b]	13.0	−0.8	12.2	14.2	−1.6	12.6
	Klamt[c]	16.9	−0.7	16.2	17.0	−1.2	15.8
	Pauling	24.0	1.9	25.9	21.5	1.6	23.1
	Pauling (scaled)[d]	18.5	1.9	20.4			
	Bondi	22.4	1.2	23.6	21.4	0.5	21.9
	Bondi (scaled)[d]	17.7	1.2	18.9			
CPCM	UA0	13.5	−2.7	10.8	14.7	−2.8	11.9
	UFF	14.7	−1.3	13.4	14.9	−1.7	13.2
	UAKS (scaled)	12.8	−0.7	12.1	13.8	−1.5	12.3
	UAHF (scaled)	13.1	−0.8	12.3	14.2	−1.5	12.7
	COSMO[e]	17.8	−0.7	17.1	18.4	−1.2	17.2
	Pauling	24.2	1.9	26.1	21.6	1.6	23.2
	Bondi	22.5	1.2	23.7	21.5	0.5	22.0
SCIPCM	0.001[f]	14.0		14.0			
	0.002[f]	14.9		14.9			
	0.00275[f]	17.4		17.4			
	0.0028[f]	22.4		22.4			

[a] Calculated at B3LYP/TZVP/Stuttgart and SVWN/TZVP/Stuttgart levels. [b] Scale factor = 1.2. [c] PCM calculation using Klamt radii (from COSMO). [d] Scale factor = 1.1. [e] COSMO as implemented in Gaussian03 (U scale factor = 1.17). [f] Isodensity value, in au.

by the PCM method. The atomic radii used are listed by type in Table 1. Graphical representations of cavity sizes and shapes (with volumes and surface areas) are shown in Figure 3 for $UO_2(H_2O)_5^{2+}$ and $UO_2(H_2O)_4^{2+}$. The UA0, UAHF, and UAKS radii are based on the United Atom Topological Model, where the oxygen and hydrogen atoms are combined at sites where they are connected via bonding. The remaining UFF, Pauling, and Bondi radii use explicit spheres on all atoms, including hydrogen, as evident in the more contoured surfaces of the cavities in Figure 3. The COSMO implemented approach in Gaussian03 uses the CPCM method and Klamt radii on all solute atoms; Klamt radii were also used to mimic the COSMO model in the PCM framework.

The correlation between the cavity size and the electrostatic contributions to the reaction free energy shown in Table 6 indicate that the primary factor governing the contribution of solvation effects to the free energy of reaction in solution is the volume of the cavities. The UA0, UFF, scaled UAHF, and scaled UAKS radii (we note that Barone et al.[65b] recommend that UAHF and UAKS radii be scaled (1.2) by default) all contain rather large spheres on the O and H atoms, thus giving larger solute cavity volumes. Generation of larger cavities results in smaller total solvation energy contributions, as the charge polarization is spread over a larger volume and the solute is thus less effectively solvated by the electrostatic field of the solvent. Additional negative nonelectrostatic contributions lower the solvation energy contribution to the free energy of solution, even further leading to free energies of reaction in solution that are too negative. The COSMO/Klamt radii for uranium and oxygen are comparable to the previous sets, but the hydrogen radius is smaller. Due to the hydrogen being on the exterior of the cavity, the effect is to decrease the cavity size and to increase the electrostatic contribution to the free energy of reaction in solution by 2−4 kcal/mol over the UA0, UFF, scaled UAHF, and scaled UAKS results. Relatively large changes in the uranium radius are energetically inconsequential, as it is buried within the center of the cavity. The Pauling and Bondi radii (unscaled) contain the most compact oxygen and hydrogen atoms of all the sets. These cavity volumes are considerably smaller than the others, which has a dramatic effect on the electrostatic contribution to the reaction free energy, as smaller cavities lead to larger positive differences in the solvation contribution to the free energy of reaction in solution. The electrostatic energy contribution to the free energy of reaction in solution is now 5.5−7.0 kcal/mol more positive than that from the COSMO/Klamt approach. These small cavities also have positive nonelectrostatic contributions, making the total solvation contribution to the free energy of reaction in solution 7−10 kcal/mol more positive than the COSMO/Klamt method, and 10−15 kcal/mol more positive than the other approaches.

It has recently been suggested that, to properly model ion cavities, scaling factors should be used to either decrease or increase the size of the radii.[71] We applied scaling factors of 1.1 to the Pauling and Bondi radii at the B3LYP/PCM level to make the cavities slightly larger. We also used unscaled UAHF and UAKS radii, because these are typically scaled by 1.2 in the literature. Scaled Pauling and Bondi radii generated slightly larger cavities, which were enough to lower the electrostatic and total solvation contributions to the free energy of reaction in solution by 5.5 and 4.7 kcal/mol, respectively, with no effect on the nonelectrostatic term. Unscaled UAHF and UAKS radii resulted in electrostatic and total solvation contributions to the free energy of reaction in solution that were 8.0 and 7.8 kcal/mol larger than results using the recommended scaled (1.2) radii. The individual electrostatic contributions to the free energy of reaction in solution for $UO_2(H_2O)_5^{2+}$, $UO_2(H_2O)_4^{2+}$, and H_2O using unscaled UAHF and UAKS radii were all significantly more negative than any of the other approaches, indicating that the smaller OH spheres may result in errant electrostatic behavior.

The SCIPCM approach is not based on atomic radii assignment, but rather a specified contour of the electron density. Figure 4 shows the variation in the electrostatic contribution to the solution energy as a function of the SCIPCM isodensity value.[72] Calculations were performed at isodensity values over the range 0.00001−0.0029 au to adequately sample the electron density. It is clear from the plot that the choice of the isodensity contour leads to significant differences in the electrostatic

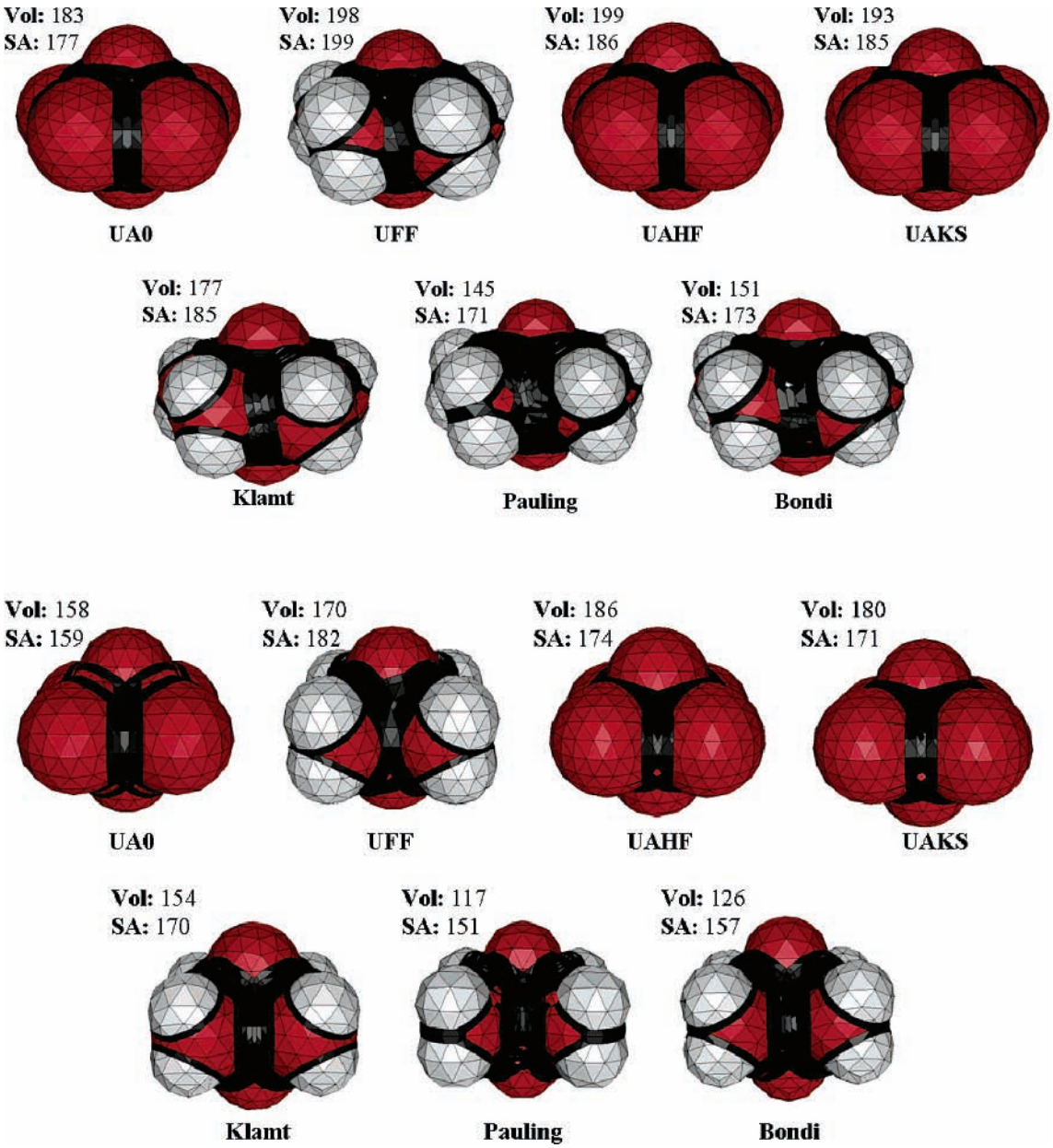

Figure 3. $UO_2(H_2O)_5^{2+}$ (top) and $UO_2(H_2O)_4^{2+}$ (bottom) cavities with volumes (Å^3) and surface areas (Å^2) at B3LYP/PCM level (with scaled UAHF and UAKS radii and unscaled Pauling and Bondi radii).

contribution to the free energy of solvation at the low and high ends of the range we chose but gives value of the electrostatic contribution that are fairly constant over the range 0.004−0.00225 au. It has been suggested that an isodensity value in the range 0.0004−0.001 au is appropriate and suitable for neutral molecules, but this is not necessarily true for anions and cations.[73] Over the contour range from 0.001 to 0.0025 au, the electrostatic contribution varies by only ∼1.6 kcal/mol and is consistent with large cavities such as that found with UA0 and UFF methods. To obtain electrostatic values that are more indicative of small cavities, isodensity values ≥0.00275 au are needed. With contours of 0.00275 and 0.0028 au, the electrostatic contributions to the free energy of solvation are 17.4 and 22.4 kcal/mol, respectively, a sharp increase in the electrostatic contribution over a narrow range of contours. If one examines the energy changes for $UO_2(H_2O)_4^{2+}$ and $UO_2(H_2O)_5^{2+}$ in going from 0.00275 and 0.0028, there is a difference of −7.5 and −2.5 kcal/mol, respectively, indicating that the isodensity contour is very sensitive for smaller volumes.

The solution free energy change for exchange reaction 1 is shown in Table 7 as a function of cavity type with the PCM model, and isodensity value with the SCIPCM model. As described above, the PCM and CPCM models give nearly identical results, so we only report the PCM results for the thermodynamic predictions. The free energy in solution for the exchange reaction, $\Delta G_{exchange}$, varies substantially and illustrates the high sensitivity of the free energy change to the methodology used to generate the cavity. $\Delta G_{exchange}$ for a given cavity was calculated by summing the gas-phase free energy from the combined MP2 and B3LYP calculations of −17.5 kcal/mol and the electrostatic and nonelectrostatic contributions from Table 6. An additional standard-state thermodynamic correction was applied to correctly model the solution chemistry of the uranyl aquo ions.[25,74] The gas-phase ΔG_{298} values reported in Table 5 are applicable only at a pressure of 1 atm. In the liquid phase (new standard state), water molecules are present at a concentration of 55.5 M, yielding a pressure of 1354 atm (from $P = \rho RT$). Each water molecule has less translational freedom, as

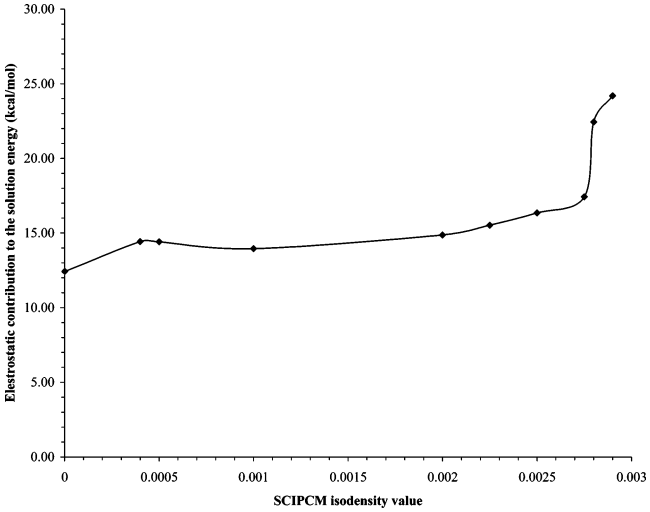

Figure 4. Variation in the electrostatic contribution to the solution energy versus SCIPCM isodensity value for the reaction $UO_2(H_2O)_4^{2+} + H_2O \leftrightarrow UO_2(H_2O)_5^{2+}$.

TABLE 7: Free Energy of Reaction in Solution (ΔG_{corr}) (kcal/mol) at the PCM and SCIPCM Levels[a]

model	cavity	$\Delta G_{exchange}$	ΔG_{corr}	$\Delta_{theory-exp}$[b]
PCM	UA0	−6.8	−11.1	−9.9
	UFF	−4.2	−8.5	−7.3
	UAKS	2.5	−1.8	−0.6
	UAKS (scaled)[c]	−5.5	−9.8	−8.6
	UAHF	2.5	−1.8	−0.6
	UAHF (scaled)[c]	−5.3	−9.6	−8.4
	Klamt	−1.3	−5.6	−4.4
	Pauling	8.4	4.1	+5.3
	Pauling (scaled)[d]	2.9	−1.4	−0.2
	Bondi	6.1	1.8	+3.0
	Bondi (scaled)[d]	1.4	−2.9	−1.7
SCIPCM	0.001[e]	−3.5	−7.8	−6.6
	0.002[e]	−2.6	−6.9	−5.7
	0.00275[e]	−0.1	−4.4	−3.2
	0.0028[e]	4.9	0.6	+1.8

[a] With respect to the MP2/aug-cc-pVQZ(+g) gas-phase free energy (−17.5 kcal/mol), including the solvation energy (electrostatic + nonelectrostatic) at the B3LYP/TZVP level and standard state correction. [b] $\Delta_{theory-exp} = \Delta G_{corr} - (-1.2)$. [c] Scale factor = 1.2. [d] Scale factor = 1.1. [e] Isodensity value, in au.

the translational entropy partition function is pressure dependent. The result is to lower the overall reaction free energy of reaction 1 by −4.3 kcal/mol. Table 7 contains the solution free energies of reaction that have been appropriately corrected for the standard state change (ΔG_{corr}).

At the PCM level, the most negative $\Delta G_{exchange}$ is predicted to occur for the UA0, UFF, scaled UAKS, and scaled UAHF methods (−4.2 to −6.8 kcal/mol). For these methods, the cavity for each of the solute species is large, leading to a smaller positive solvation contribution to the free energy of reaction in solution and the reaction free energy in solution is dominated by the gas-phase exothermicity. Addition of the standard state correction leads to results that are even more exothermic for the final free energy of reaction in solution, ΔG_{corr}, and have a greater deviation from the experimental value when using the UA0, UFF, scaled UAHF, and scaled UAKS cavities. Thus large solute cavities are not appropriate for the description of the uranyl aquo ion water exchange chemistry. The disagreement with experiment ($\Delta_{theory-exp}$) is between −7.3 and −9.9 kcal/mol in these cases. The PCM model using the Klamt radii yields a slightly negative (−1.3 kcal/mol) exchange free energy, and the best agreement with the experimental HEXS results (−1.2 kcal/mol). However, when corrected for the new standard state, $\Delta_{theory-exp}$ becomes −4.4 kcal/mol in this case. The results for $\Delta G_{exchange}$ with unscaled Pauling and Bond radii are in contrast with the other predefined radii sets. Because $\Delta G_{exchange}$ is positive (8.4 and 6.1 kcal/mol, respectively), the solvation contribution dominates the gas-phase free energy, giving an endothermic result. This is consistent with smaller cavities and larger solvation energies. After the standard state corrections, the Bondi radii provide a result that is in relatively good agreement with experiment, with a value of $\Delta G_{corr} = 1.8$ kcal/mol and a deviation of +3.0 kcal/mol. Use of the Pauling radii leads to an energy change that is too positive, disagreeing with experiment by +5.3 kcal/mol.

If the Pauling and Bondi radii are scaled by 1.1, leading to slightly larger cavities, the results are in even better agreement with experiment. The corrected solution free energies are −1.4 and −2.9 kcal/mol, yielding $\Delta_{theory-exp}$ of −0.2 and −1.7 kcal/mol, respectively. Similarly, unscaled UAHF and UAKS provide corrected solution free energies of −1.8 kcal/mol in both cases, an improvement of ∼8 kcal/mol over the recommended scaled results, leading to $\Delta_{theory-exp} = -0.6$ kcal/mol. Scaling the radii is consistent with other approaches reported in the literature[71] and is important in modeling the solvation effects on the energetics of reaction 1. Overall, it is apparent that smaller cavities (larger solvation energy corrections) are needed to predict the equilibrium free energy for reaction 1 in solution. The results are very dependent upon the choice of the radii and must be carefully chosen. Explicit radii sets were used to examine the effects of small, incremental changes in radii on the reaction energetics and these results are included as Supporting Information. We noted that small changes in the O and H radii can be used to fine-tune the energetics but that there was essentially no effect for any reasonable value for the U radius.

Clearly, the most desirable way to predict these solvation effects is a method that does not depend on assigning predefined radii to the atoms. The SCIPCM is such an approach, and the variation in the electrostatic contribution with SCIPCM isodensity value was presented in Figure 4. It is apparent from the above discussion that more compact solute cavities are appropriate for studying the species in reaction 1. Using an isodensity value of 0.001 au gave results that were similar to those obtained with the UA0 and UFF cavities, and thus the electron density contour defining the cavity in this manner was too small, giving a cavity that was too large. Increasing the size of the contour to 0.002 au gave results that were consistent with the Klamt/COSMO approach and were also in error, by −4.5 kcal/mol. However, as shown in Table 7, a contour in the range 0.00275−0.0028 yielded results that were more consistent with the experimental value, at −4.4 and 0.6 kcal/mol, respectively. Because these free energies are essentially upper and lower bounds to the chemical accuracy desired, it is then apparent that the appropriate contour values lie somewhere in this range. However, in this region, the electrostatic contribution varies significantly over a small range of contours. These results suggest that a value of 0.001 au may not be not suitable for cations, although it may work well for most neutral species, and a larger contour (smaller cavity) is necessary just as found for anions in predicting pK_a's for acids.[73] Thus, benchmarking of the SCIPCM method requires a precise knowledge of experimental solvation free energies to calibrate isodensity values. This will help to broaden the applicability of the SCIPCM approach to more types of species, notably dications.

Cluster Geometries and Thermodynamics. On the basis of the above results, we decided to look at larger clusters where part of the second solvation shell is present. To examine the effect of explicit second sphere solvent molecules on the geometries, as well as the water exchange energetics, of the $UO_2(H_2O)_4^{2+}$ and $UO_2(H_2O)_5^{2+}$ ions, the clusters $UO_2(H_2O)_4(H_2O)_8^{2+}$, $UO_2(H_2O)_4(H_2O)_{10}^{2+}$, $UO_2(H_2O)_4(H_2O)_{11}^{2+}$, $UO_2(H_2O)_5(H_2O)_7^{2+}$, and $UO_2(H_2O)_5(H_2O)_{10}^{2+}$ were optimized at the B3LYP level with the previously defined basis sets and ECP. Vibrational frequencies were calculated to ensure that the located structures were minima (zero imaginary frequencies). In the first and fifth clusters, two second sphere water molecules were assigned to hydrogen bond to each of the primary sphere water molecules, whereas in the remaining clusters this 2:1 water stoichiometry was not maintained, resulting in both a deficit and excess of water in this sphere. For these other clusters, the water molecules were initially assigned in typical hydrogen bonding positions. Although our inclusion of outer sphere water molecules is likely to underestimate the actual number present in solution, it should provide a more realistic picture of solution effects on the geometry about the uranyl ion. The structures of the $UO_2(H_2O)_4(H_2O)_8^{2+}$, $UO_2(H_2O)_4(H_2O)_{10}^{2+}$, and $UO_2(H_2O)_4(H_2O)_{11}^{2+}$ clusters are shown in Figure 5 and the $UO_2(H_2O)_5(H_2O)_7^{2+}$ and $UO_2(H_2O)_5(H_2O)_{10}^{2+}$ clusters are shown in Figure 6. As indicated by the dashed lines, hydrogen bonding plays a significant role in the interactions between the first and second hydration spheres, as well as within the second shell. The structural parameters and uranyl vibrational frequencies of all five clusters are listed in Tables 3 and 4.

In the three tetraaquo clusters $UO_2(H_2O)_4(H_2O)_8^{2+}$, $UO_2(H_2O)_4(H_2O)_{10}^{2+}$, and $UO_2(H_2O)_4(H_2O)_{11}^{2+}$, the U═O bonds lengths are lengthened by 0.019, 0.023, and 0.024 Å, respectively, compared to the B3LYP gas-phase structure of $UO_2(H_2O)_4^{2+}$. This is indicative of more charge transfer to the uranium center, causing a lengthening of the oxo bonds (see below). In addition, the equatorial bonds are shortened by 0.067, 0.073, and 0.075 Å due to stronger interactions with the uranyl as a result of the second shell effects. The uranyl symmetric and asymmetric stretches are lowered by about 40−50 and 37−50 cm^{-1}, respectively, in the larger clusters, consistent with the lengthening of the U═O bonds, and are now much closer to the experimental values. In the $UO_2(H_2O)_4(H_2O)_8^{2+}$ cluster, there is no observable hydrogen-bonding present between water molecules in the second shell, due to the open nature of the cluster, and the overall shape of the cluster is approximately cubic. Thus, no significant rearrangement of the $UO_2(H_2O)_4^{2+}$ core occurs, and the symmetry is only reduced to approximately D_4 from D_{4h}. In the two larger clusters, however, the larger number of water molecules in the second shell leads to hydrogen bonding in the second shell, which causes the core to distort slightly, resulting in approximate C_2 and C_i symmetry for the core, respectively. The uranyl moiety remains linear in each cluster, with only small deviations due to asymmetries caused by the hydrogen bonding between the first and second solvation shells. The average U−O distance to water molecules in the second shell varies from 4.48(1) to 4.43(15) to 4.45(9) Å in the three respective clusters. The smallest variation in this length occurs for $UO_2(H_2O)_4(H_2O)_8^{2+}$, whereas larger variations are found for the latter two clusters. The pentaaquo clusters $UO_2(H_2O)_5(H_2O)_7^{2+}$ and $UO_2(H_2O)_5(H_2O)_{10}^{2+}$ can be directly compared with the condensed-phase experimental data listed in Table 3. The latter cluster is the most realistic, as the HEXS results suggest 10 water molecules in the second shell at an average distance of 4.50 Å. In the two clusters, the average

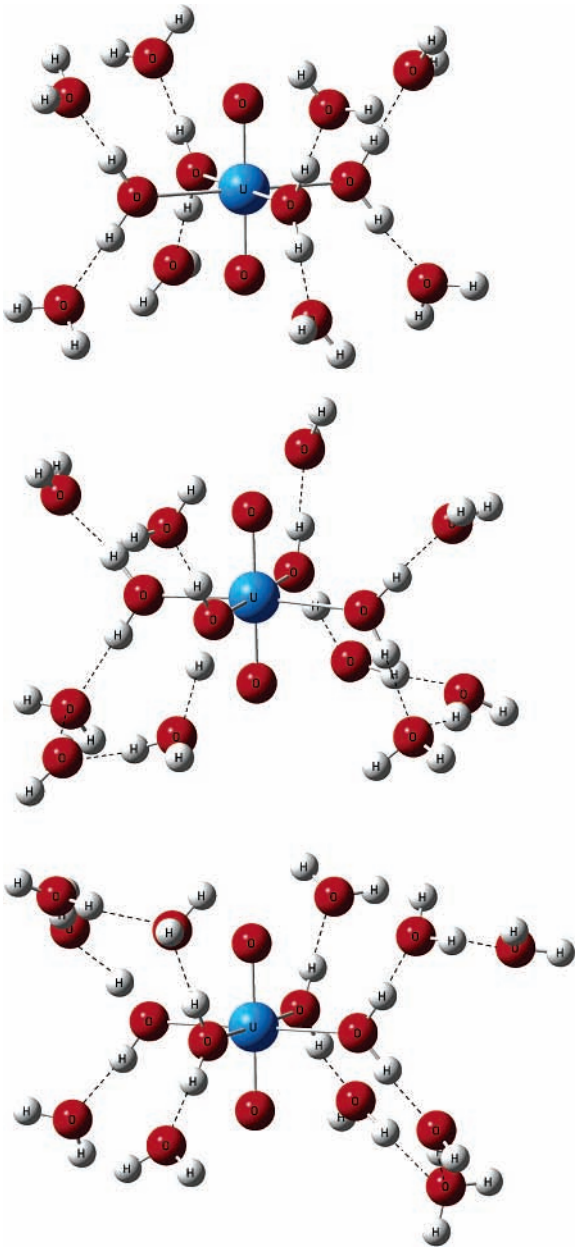

Figure 5. Optimized gas-phase structures (B3LYP/TZVP/Stuttgart) of $UO_2(H_2O)_4(H_2O)_8^{2+}$, $UO_2(H_2O)_4(H_2O)_{10}^{2+}$, and $UO_2(H_2O)_4(H_2O)_{11}^{2+}$ ion clusters, with hydrogen bonds indicated by dashed lines.

$U-O_{second}$ distances are 4.45(16) and 4.64(19) Å, respectively, which agree well with the HEXS measured value. In both clusters, the U═O bond is lengthened compared to that in the gas-phase structure of $UO_2(H_2O)_5^{2+}$ by 0.015 and 0.019 Å, respectively, and both values are in excellent agreement with HEXS and EXAFS values of 1.766 and 1.76 Å. The calculated values show larger differences in comparison to the 1.783 Å EXAFS value[8b] and the solution XRD[12] results, suggesting a poor refinement of the bond length in these cases. Lengthening of the oxo bond is again consistent with enhanced charge transfer due to waters in the second shells (see below).

The addition of the second sphere water molecules has a dramatic effect on the structure of the $UO_2(H_2O)_5^{2+}$ core. Significant hydrogen bonding occurs, which in the $UO_2(H_2O)_5(H_2O)_{10}^{2+}$ cluster, results in a partitioning into two distinct structural regions. First, there is a region encompassing two equatorial oxygen atoms and four second shell waters that is partitioned into a pyramid-like structure with a well-defined

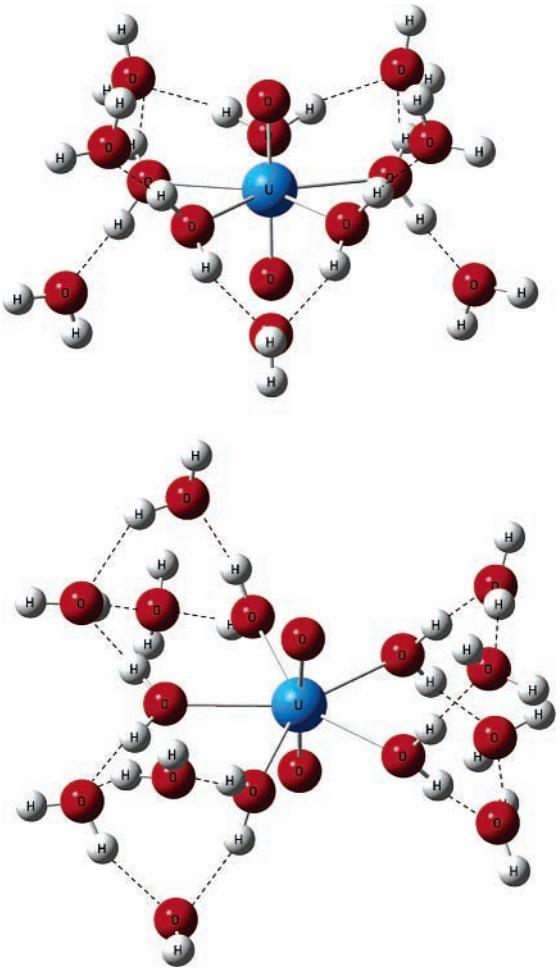

Figure 6. Optimized gas-phase structures (B3LYP/TZVP/Stuttgart) of $UO_2(H_2O)_5(H_2O)_7^{2+}$, and $UO_2(H_2O)_5(H_2O)_{10}^{2+}$ ion clusters, with hydrogen bonds indicated by dashed lines.

shape. Second, there is a region comprising the remaining first and second sphere waters that encompasses an entire hemisphere of the overall cluster and is linked together via hydrogen-bonding. Whereas, in the isolated $UO_2(H_2O)_5^{2+}$ ion, all of the water molecules are nearly parallel with the uranyl axis, giving it D_5 symmetry, here one water molecule is now nearly perpendicular to the uranyl axis and there is significant twisting of the remaining water molecules, all of which are due to strong hydrogen bond effects, giving it approximate C_2 symmetry. Short hydrogen bonds (H−O- - -H) are present that range from 1.64 to 1.97 Å and exist between second sphere oxygen atoms and first sphere hydrogen atoms. A similar effect is observed in the $UO_2(H_2O)_5(H_2O)_7^{2+}$ cluster, although the smaller number of water molecules in the second shell results in enhanced strain on the core structure and stronger twisting of four of the bound water molecules, with a fifth perpendicular water as in the previous case (approximate C_s symmetry).

In the clusters $UO_2(H_2O)_5(H_2O)_7^{2+}$ and $UO_2(H_2O)_5(H_2O)_{10}^{2+}$ the equatorial region has four short bonds and one relatively long bond in each case. The former bonds are shortened compared to the gas phase by 0.058 and 0.067 Å, respectively, and are in excellent agreement with the experimental values (within 0.01−0.03 Å). However, one of the equatorial bonds in each cluster is lengthened significantly with respect to the other four at 2.546 and 2.525 Å, respectively. This is a strong indication that inclusion of the second sphere waters has a destabilizing effect on the $UO_2(H_2O)_5^{2+}$ core and supports the conclusion based on the HEXS measurement that the tetraaquo species may contribute significantly to the solution equilibrium. In the clusters, the frequencies for the symmetric uranyl stretches are lowered by 28 and 40 cm^{-1} as compared to the B3LYP gas-phase values, and the asymmetric uranyl stretches are lowered by 32 and 34 cm^{-1}, respectively. The agreement with experiment is improved, although there is still a difference of about 50−60 cm^{-1} in the symmetric stretch and 45−47 cm^{-1} in the asymmetric stretch. The differences from experiment are due to our neglect of anharmonic contributions, the functional that was used, and additional solvation effects. The experimental HEXS spectrum shows a peak at 4.50 Å indicative of 10 water molecules in the second shell, which is in relatively good agreement with the $UO_2(H_2O)_5(H_2O)_{10}^{2+}$ cluster results at 4.6 Å, although the high standard deviation of the calculated values indicates strong fluctuations in this shell. Overall, the explicit inclusion of outer sphere solvent molecules provides a more realistic description of the uranyl aquo ion system that is otherwise absent in the gas-phase results when only the first solvation shell is included.[75] For all of the clusters studied, we note that there is a lack of hydrogen-bonding to the uranyl oxygen atoms. In all cases, the second sphere water molecules form an exclusionary space in the region of axial oxygen atoms with their hydrogen atoms pointed up, thus preventing water molecules from entering and interacting with the oxo atoms. Instead, additional waters would likely prefer to form hydrogen bonds with the second sphere water molecules. This is supported by the molecular dynamics simulation of the uranyl−water system of Hagberg et al.[41] They noted that no hydrogen bonding is found between the uranyl oxygen atoms and water molecules during the course of the simulation. In our $UO_2(H_2O)_4(H_2O)_{11}^{2+}$ cluster, one of the second shell water molecules effectively starts a "third" solvation shell by hydrogen bonding to a second sphere water rather than forming an interaction with an oxo ligand.

In the $UO_2(H_2O)_5(H_2O)_{10}^{2+}$ cluster, charge-transfer effects account for the movement of 0.66 e to the uranyl (+1.34 group charge), 0.14 e more than in $UO_2(H_2O)_5^{2+}$, based on NBO calculations. This clearly shows that additional charge transfer from the inner tightly bound first solvation shell can be induced by the presence of a second hydration sphere. The 10 water molecules in the second shell have individual positive charges of between +0.022 and +0.045, with a net charge of +0.369. In the $UO_2(H_2O)_4(H_2O)_8^{2+}$ cluster 0.65 e are transferred to the uranyl (+1.37 group charge), 0.16 e more than in the $UO_2(H_2O)_4^{2+}$. The eight water molecules in the second shell acquire a net positive charge of +0.392. In the remaining clusters, $UO_2(H_2O)_4(H_2O)_{10}^{2+}$, $UO_2(H_2O)_4(H_2O)_{11}^{2+}$, and $UO_2(H_2O)_5(H_2O)_7^{2+}$, the uranyl group charges were +1.34, +1.34, and +1.37, respectively. This suggests that molecular dynamics simulations of these ions in solution should include charge-transfer and polarizability effects.[76] In addition, our charge-transfer results confirm the average amount of charge transfer assumed by Soderholm et al.[18b] in fitting the HEXS results.

As discussed above, the addition of a second hydration sphere to $UO_2(H_2O)_4^{2+}$ and $UO_2(H_2O)_5^{2+}$ greatly improves the agreement of the geometric parameters of the core uranyl aquo ion with experiment. Also, the NBO charges show an impact on the charge distribution, and hence the energetics, in the core due to the presence of outer sphere water molecules. These additional water molecules, analogous to the inclusion of a continuum dielectric, are effectively polarizing the charge distribution of the solute. The energetics of the water exchange reaction as shown in reaction 1 with the larger clusters were calculated using both the B3LYP with the TZVP and Stuttgart/ECP basis without g functions energies and single point MP2

TABLE 8: Individual Energy Component Contributions (kcal/mol) for Reactions 2−7 at the B3LYP and MP2[a] Levels

rxn	method	ΔE_{elec}	ΔZPE	ΔE_0	ΔE_{298}	ΔH_{298}	$-T\Delta S_{298}$	ΔG_{298}	$\Delta G_{exchange}$ (electrostatic)[b]	SS corr[c]	$\Delta G_{exchange}$ (nonelectrostatic)[b]	ΔG_{corr} (electrostatic)[d]	ΔG_{cor} (full)[e]
2	B3LYP	−45.6	13.2	−32.4	−36.2	−38.0	42.0	4.0	31.4	−12.9	−9.0	22.5	13.5
3	B3LYP	−28.0	7.4	−20.6	−23.7	−24.3	25.2	0.9	17.0	−1.4	−7.4	16.5	9.1
4	B3LYP	−19.1	6.4	−12.7	−14.8	−15.4	18.2	2.8	13.7	−4.3	−7.0	12.2	5.2
5	B3LYP	−13.3	4.1	−9.2	−11.4	−11.4	11.9	0.5	10.2	+2.2	−6.6	12.9	6.3
6	B3LYP	−1.5	3.4	1.9	0.0	0.0	7.5	7.5	0.0	0.0	−4.7	7.5	2.9
7	B3LYP	−3.1	4.5	1.4	−1.1	−1.1	10.7	9.6	3.0	0.0	−6.9	12.6	5.7
2	MP2	−51.7	12.9	−38.8	−42.7	−44.5	42.1	−2.4	31.4	−12.9	−9.0	16.1	7.1
3	MP2	−35.6	7.4	−28.1	−31.2	−31.8	25.1	−6.7	17.0	−1.4	−7.4	8.9	1.5
4	MP2	−25.5	6.3	−19.3	−21.4	−22.0	18.2	−3.8	13.7	−4.3	−7.0	5.6	−1.4
5	MP2	−20.4	4.2	−16.2	−18.4	−18.4	12.1	−6.3	10.2	+2.2	−6.6	6.1	−0.5
6	MP2	−6.9	3.4	−3.5	−5.4	−5.4	7.5	2.1	0.0	0.0	−4.7	2.1	−2.5
7	MP2	−10.9	4.5	−6.4	−8.9	−8.9	10.7	1.8	3.0	0.0	−6.9	4.8	−2.1

[a] MP2 with aug-cc-pVTZ on H, O and Stuttgart small core basis set (w/ RECP) plus g functions on U. [b] From PCM/UA0 solvation model performed at the B3LYP/TZVP/Stuttgart level. [c] Standard state correction (see ref 78). [d] Total corrected free energy including only electrostatic contribution to solvation. [e] Total corrected free energy including full solvation correction.

energies with the modified Stuttgart 60 e basis and RECP on U including g functions, and aug-cc-pVTZ basis sets on H and O. Such calculations minimize the reliance on the SCRF approach, which can predict values only to within ±2−3 kcal/mol. The reactions of the clusters are given by the following reactions (overall the stoichiometry is the same as that in reaction 1):

$$UO_2(H_2O)_4(H_2O)_8^{2+} + 3H_2O \rightleftharpoons UO_2(H_2O)_5(H_2O)_{10}^{2+} \quad (2)$$

$$UO_2(H_2O)_4(H_2O)_8^{2+} + (H_2O)_3 \rightleftharpoons UO_2(H_2O)_5(H_2O)_{10}^{2+} \quad (3)$$

$$UO_2(H_2O)_4(H_2O)_{10}^{2+} + H_2O \rightleftharpoons UO_2(H_2O)_5(H_2O)_{10}^{2+} \quad (4)$$

$$UO_2(H_2O)_4(H_2O)_{10}^{2+} + (H_2O)_2 \rightleftharpoons UO_2(H_2O)_5(H_2O)_{10}^{2+} + H_2O \quad (5)$$

$$UO_2(H_2O)_4(H_2O)_8^{2+} \rightleftharpoons UO_2(H_2O)_5(H_2O)_7^{2+} \quad (6)$$

$$UO_2(H_2O)_4(H_2O)_{11}^{2+} \rightleftharpoons UO_2(H_2O)_5(H_2O)_{10}^{2+} \quad (7)$$

Reactions 2 and 3 involve the addition of three water molecules to the $UO_2(H_2O)_4(H_2O)_8^{2+}$ cluster to form $UO_2(H_2O)_5(H_2O)_{10}^{2+}$ and are treated as individual water molecules in reaction 2, and as the water trimer in reaction 3. In these systems, the change in the number of free particles that must be treated is reduced from three to one. Reactions 4 and 5 involve the addition of one water molecule to $UO_2(H_2O)_4(H_2O)_{10}^{2+}$ to form $UO_2(H_2O)_5(H_2O)_{10}^{2+}$. In reaction 4, the reactant water is treated as discrete entity, whereas in the reaction 5 it is treated as a dimer, with the corresponding formation of a monomer product. In reaction 5, there is no net change in the number of free particles from reactants to products, and the reaction energy includes the hydrogen bond energy of the dimer.[77] Reactions 6 and 7 are rearrangement (intramolecular isomerization) reactions, which do not depend on water molecules or different size clusters in the reaction. These reactions involve an intramolecular transfer of a water molecule from the second sphere to the primary sphere as a ligand bound to uranium.

Table 8 contains the individual energy components used to predict the reaction energetics from reactions 2−7. In all cases, the gas-phase reaction enthalpies at 298 K are distinctly exothermic (thermoneutral for reaction 6 at the B3LYP level), with the MP2 values being more negative than the B3LYP values in all cases, consistent with the gas-phase results in Table 5. However, the entropy correction at 298 K to the gas-phase free energy change for the cluster reaction results in a substantial shift of the values in a positive direction, pushing the reactions to be less favorable. For the B3LYP values, all of the reactions become endothermic and the MP2 reactions in a number of cases approach and bracket a value of 0. There are clearly large entropy contributions to the free energy when the number of particles in the reaction changes. In addition, an important contribution to the entropy of the cluster in each case is the vibrational entropy due to the large number of low vibrational modes that these "floppy" clusters have as the second shell is quite fluxional, i.e., nonrigid. We note that our treatment of the entropy based on the harmonic oscillator approximation could lead to some errors in the calculated entropies for a given cluster but that the similar cluster sizes will cause some of these errors to cancel in predicting the entropy change for the reaction. In addition, there could be a number of geometric isomers for a given structure that are low in energy that should be included. However, the fact that we obtain quite good agreement with the experimental results suggests that we are not making a substantial error in using the lowest energy structure and the frequencies corresponding to that structure.

The solvation energies were obtained from an SCRF calculation on the optimized gas-phase structures as described above. For the large uranyl clusters, a standard PCM model (using UA0 radii) was deemed sufficient to account for solvation effects because the large size of the cluster should effectively cancel out dramatic effects that were observed in the smaller core structures. The PCM prediction of the free energy of solvation of the water molecule resulted in a solvation energy of −7.3 kcal/mol, in reasonable agreement with the experimental value of −6.3 kcal/mol.[74a] As shown in Table 8, the electrostatic solvation energy contribution is largest for reactions 2−5 due to the necessity of treating the excess free particles in reactions 2−4 and the difference between the water molecule and the dimer in reaction 5. Electrostatic solvation effects approximately cancel in reactions 6 and 7, and are almost essentially negligible in each case, but are included for consistency. As shown in Table 8, the nonelectrostatic component actually accounts for a large fraction of the overall solvation energy contribution, and are thus more important than for reaction 1. It is also noted that the cavitation and dispersion terms are likely to be negligible for uranium in these larger clusters as it is completely enclosed. The ΔG_{corr} values correspond to the sum of ΔG_{298} and the electrostatic and/or the nonelectrostatic solvation contributions (see Table 8, footnotes d and e), as well as the standard state correction described above when there is a net change in the number of free particles or water cluster size in the reaction.[78]

TABLE 9: Solvation Free Energy (kcal/mol) of the Uranyl Cation Using the SCIPCM Approach and a 0.001 au Contour[a]

rxn	method	ΔE_{elec}	ΔZPE	ΔE_0	ΔE_{298}	ΔH_{298}	$-T\Delta S_{298}$	ΔG_{298}	$\Delta\Delta G_{solv}$ (electrostatic)[b]	SS corr[c]	ΔG_{corr}[d]
8	B3LYP	−192.6	0.7	−192.0	−191.4	−192.0	12.2	−179.8	−225.9	−1.1	−406.8
9	B3LYP	−223.9	9.3	−214.6	−215.2	−217.8	39.0	−178.8	−208.4	−17.2	−404.4
10	B3LYP	−207.2	−0.4	−207.6	−206.3	−206.9	11.6	−195.3	−217.1	−0.9	−413.3
11	B3LYP	−248.4	10.3	−238.1	−237.9	−240.8	46.3	−194.5	−194.5	−21.5	−410.5
8	MP2	−195.1	0.6	−194.5	−193.9	−194.5	12.0	−182.5	−225.9	−1.1	−409.5
9	MP2	−223.0	9.2	−213.8	−214.4	−216.7	38.6	−178.1	−208.4	−17.2	−403.7
10	MP2	−213.3	−0.2	−213.5	−212.3	−212.9	12.0	−200.9	−217.1	−0.9	−418.9
11	MP2	−249.9	10.4	−239.4	−239.3	−242.3	46.7	−195.6	−194.5	−21.5	−411.5

[a] Nonelectrostatic contribution neglected because it is approximately negligible (−1.6 to +3.6 kcal/mol from PCM analysis). SCIPCM contributions were obtained at the B3LYP/TZVP/Stuttgart level. [b] Solvation contribution of water cluster and uranyl−water cluster. [c] Standard state correction (see ref 78). [d] Total corrected free energy including electrostatic solvation correction.

TABLE 10: Solvation Free Energy (kcal/mol) of the Uranyl Cation Using the PCM Approach[a]

rxn	method	ΔE_{elec}	ΔZPE	ΔE_0	ΔE_{298}	ΔH_{298}	$-T\Delta S_{298}$	ΔG_{298}	$\Delta\Delta G_{solv}$ (electrostatic)[b]	SS corr[c]	$\Delta\Delta G_{solv}$ (nonelectrostatic)[d]	ΔG_{corr}[e]
12	B3LYP	−259.7	−10.0	−269.6	−262.8	−263.4	−10.6	−274.0	−149.0	−0.4	11.8	−411.6
13	B3LYP	−261.1	−6.6	−267.7	−262.8	−263.3	−3.1	−266.4	−149.0	−0.4	7.2	−408.7
14	B3LYP	−266.6	−9.4	−276.0	−269.7	−270.3	−9.7	−280.0	−142.7	−0.3	11.0	−412.1
15	B3LYP	−269.7	−5.0	−274.6	−270.8	−271.4	+1.0	−270.4	−139.4	−0.3	4.1	−406.0
12	MP2	−256.6	−10.0	−266.6	−259.7	−260.3	−10.6	−270.9	−149.0	−0.4	11.8	−408.5
13	MP2	−263.5	−6.6	−270.0	−265.1	−265.7	−3.1	−268.8	−149.0	−0.4	7.2	−411.0

[a] PCM/UA0 contributions obtained at the B3LYP/TZVP/Stuttgart level. [b] Solvation contribution of water cluster and uranyl-water cluster. [c] Standard state correction (see ref 78). [d] Included because not negligible. [e] Total corrected free energy including full solvation correction.

In all cases, the full corrected free energy change, ΔG_{corr}(full), at the B3LYP level for all of the reactions is too positive with respect to the experimental value of −1.2 kcal/mol. The B3LYP results are too positive, consistent with the gas-phase values reported in Table 5 and are due to a gas-phase value of ΔE_{elec} that is too positive. The MP2 results are in much better agreement with the experimental value. In reaction 2, the gas-phase free energy is negative but becomes too positive when corrected for solvation and pressure, indicative of the difficulty in treating the large number of free reactant particles in this case. The corrected reaction free energies of reactions 3−5 are in much better agreement with the experimental value with differences of +2.7, −0.2, and +0.7 kcal/mol, respectively. The latter two are within chemical accuracy of ±1 kcal/mol. In these reactions, the free particle problem is reduced to only one, making its treatment more tractable. Overall, these results suggest that our treatment of the solvation of the particles and the use of pressure correction is adequate in these cases (except reaction 2) and is providing a realistic picture of the chemistry involved. However, if larger water clusters or more free particles are used as variations on reactions 4 and 5, larger errors are found and such an approach is not recommended.

The rearrangement reactions 6 and 7 avoid the need to treat free particle solvation and the standard state correction and minimize differential solvation effects due to the similarities in size of the clusters. As shown in Table 8, the full corrected reaction free energies for these rearrangements are in excellent agreement with experiment, differing by only −1.3 and −0.9 kcal/mol, respectively. If only the gas-phase reaction energies are considered, the discrepancy with experiment is +3.3 and +3.0 kcal/mol, respectively In these cases, the electrostatic contribution is actually quite small, and only the nonelectrostatic contribution is important, pushing the reactions in the proper direction (more negative). In the rearrangement reactions, as the number of water molecules increases, the results are converging to the experimental value of −1.2 kcal/mol. Accounting for solvation effects is important in reactions 2−5 where the gas-phase reaction free energies are too negative, and solvation of the small water molecules and water clusters contributes significantly to moderating the reaction energies. The results for reaction 7 also support the presence of 10 water molecules in the second coordination sphere as observed in the HEXS experimental results, further demonstrating that our model is providing a reasonable picture of the solvation shells about the uranyl ion. These results are not consistent with those of Spencer et al.[28] ($\Delta G = -7.2$ kcal/mol), Hay et al.[31] ($\Delta G = -6.5$ kcal/mol), and Bühl et al.[42] ($\Delta A = -8.7$ kcal/mol) who report substantially too negative exchange reaction free energies. This can be attributed to the use of molecular cavitites that are too large for the first two. The CPMD results of Bühl et al. are too negative, potentially due to inadequate sampling. On the basis of their BLYP gas-phase electronic energy of −20.6 kcal/mol, it is highly unlikely that a free energy of −8.7 kcal/mol is a converged result, because the use of both large and small cavities in a PCM framework (see Table 6) would result in free energies of roughly 3−12 kcal/mol with respect to their gas-phase value, which differs from our highest level MP2 value by more than 6 kcal/mol.

An important consequence of the results from reactions 6 and 7 is the apparent unimportance of bulk solvation effects in describing the energetics of the uranyl water exchange reaction. In Table 5, the gas-phase MP2 reaction free energy change was predicted to be −17.5 kcal/mol. Inclusion of a only a single shell of water molecules in the second sphere (although $UO_2(H_2O)_4(H_2O)_{11}^{2+}$ contains what can be considered one-third shell water molecule) increases the gas-phase reaction free energy by 19.6 and 19.3 kcal/mol, respectively, accounting for most of the solvation effects. In fact, if one looks at the MP2 ΔG_{298} values in Table 8, all of the reactions are in qualitative agreement with the experimental value, with the maximum being only −5.5 kcal/mol. This strongly suggests that solvation effects beyond the second shell are not that important for describing the energetics of reaction 1. Because the actual energy difference is so small, the SCRF approach can lead to both underestimates and overestimates of the reaction energy.

The fact that these reactions representing predominantly a cluster approach to the prediction of the energetics of reaction 1 are only slightly favored (in most cases) is consistent with

the destabilization of the $UO_2(H_2O)_5^{2+}$ by the second solvation shell, as indicated by a lengthening of one of the $U-OH_2$ equatorial bonds. Thus the electrostatic attraction of the dication for the stabilizing water ligands must compete with the effects of hydrogen bonding between the water molecules in solution. The steric crowding in $UO_2(H_2O)_5^{2+}$ is not observed in $UO_2(H_2O)_4^{2+}$ as there is less crowding in the equatorial plane. The balance between steric repulsion, electrostatic attraction, and hydrogen bonding is why the tetraaquo ion accounts for 14% of the population in aqueous solution. In addition, the lack of any observed interaction of the water molecules in the second shell with the oxo ligands is consistent with our structures, as such an interaction should affect the reaction energetics, and this is not observed.

Solvation Free Energy of the Uranyl Ion. Tables 9 and 10 contain an evaluation of the solvation free energy of the bare uranyl dication at the B3LYP/TZVP/Stuttgart and MP2 (aug-cc-pVTZ on H, O and Stuttgart with g functions on U) levels based on the energies of the water clusters. We used the following reactions for this prediction

$$UO_2^{2+} + (H_2O)_4 \rightarrow UO_2(H_2O)_4^{2+} \quad (8)$$

$$UO_2^{2+} + 4H_2O \rightarrow UO_2(H_2O)_4^{2+} \quad (9)$$

$$UO_2^{2+} + (H_2O)_5 \rightarrow UO_2(H_2O)_5^{2+} \quad (10)$$

$$UO_2^{2+} + 5H_2O \rightarrow UO_2(H_2O)_5^{2+} \quad (11)$$

$$UO_2^{2+} + (H_2O)_{12} \rightarrow UO_2(H_2O)_4(H_2O)_8^{2+} \quad (12)$$

$$UO_2^{2+} + (H_2O)_{12} \rightarrow UO_2(H_2O)_5(H_2O)_7^{2+} \quad (13)$$

$$UO_2^{2+} + (H_2O)_{15} \rightarrow UO_2(H_2O)_4(H_2O)_{11}^{2+} \quad (14)$$

$$UO_2^{2+} + (H_2O)_{15} \rightarrow UO_2(H_2O)_5(H_2O)_{10}^{2+} \quad (15)$$

based on our previous supermolecule/continuum approach to the prediction of the free energies of solvation of small ions.[26] We used water clusters (instead of discrete water molecules) to keep the right- and left-hand sides of the reaction comparable in size in terms of the cluster, although we do include individual water molecules at the SCIPCM level (reactions 9 and 11) for comparison. The SCIPCM solvation model with an isodensity value of 0.001 au was used to predict the reaction energies for reactions 8−11. At the B3LYP level, the free energies of solvation of the uranyl dication fall in the range −404.4 to −413.3 kcal/mol, with an average value of −408.8 ± 3.9 kcal/mol. At the MP2 level, the free energies fall in the range −403.7 to −418.9 kcal/mol, with an average value of −410.9 ± 6.3 kcal/mol. The overall average value within the SCIPCM approach was −409.8 ± 5.0 kcal/mol. Our values for reactions 9 and 11 are not consistent with the results of Shamov and Schreckenbach,[48] who reported a value of −383.9 kcal/mol for the uranyl cation using the $UO_2(H_2O)_5^{2+}$ complex and discrete waters from a combined all electron-ZORA-PBE/COSMO approach. However, Shamov and Schreckenbach note that this low value is due to an approach that underestimates the estimated experimental value by 30−40 kcal/mol as well as our computational results. Our computational results are consistent with the value of −413.5 kcal/mol obtained at the SC-ECP−B3LYP/CPCM level by Shamov and Schreckenbach. Our average value of −409.8 ± 5.0 kcal/mol is in excellent agreement with a recently derived value of −421 ± 15 kcal/mol[50,51] for the free energy of solvation of the uranyl ion, which reduces the error bars from the earlier experimental value of −402 ± 60 kcal/mol.[39] Both computational and experimental values show that the earlier derived experimental value of −322 ± 5 kcal/mol for the free energy of solvation is too high.[40]

Due to difficulties in converging SCIPCM calculations on the larger uranyl cluster, the remaining reactions (12)−(15) (Table 10) were modeled with PCM solvation using UA0 radii. At the B3LYP level, the free energies of solvation ranged from −406.0 to −412.1 kcal/mol, with an average value of 409.6 ± 2.9 kcal/mol. Due to the excellent agreement between B3LYP and MP2 in nearly all instances, MP2 calculations were performed only for the $(H_2O)_{12}$ cluster reaction. These values were −408.5 and −411.0 kcal/mol for reactions 12 and 13, respectively, averaging to −409.8 ± 1.8 kcal/mol. The overall average value with the PCM approach was −409.7 ± 2.3 kcal/mol. Between both the SCIPCM and PCM methods (at B3LYP and MP2 level), the average uranyl free energy was calculated to be −409.8 ± 3.9 kcal/mol, indicating that both methods are in excellent agreement and provide a narrow range of values that are consistent with the best experimental value of −421 ± 15 kcal/mol. Our values agree well with those of Shamov and Schreckenbach who used $UO_2(H_2O)_5(H_2O)_7^{2+}$, $UO_2(H_2O)_5(H_2O)_{10}^{2+}$, and $UO_2(H_2O)_5(H_2O)_{12}^{2+}$ clusters and obtained values of −407.8, −415.9 and −415.6 kcal/mol, respectively, and recommend a value of −413.5 kcal/mol. Our results should provide an upper bound to the free energy of solvation so we can state that the free energy of solvation of the uranyl ion is ≤−410 ± 4 kcal/mol using both first and second hydration sphere models. This result is consistent with the latest experimental estimates as well as those of Shamov and Schreckenbach.[48] Our results with the SCIPCM model may be converged at the first solvation shell consistent with what has been previously found for the free energies of solvation[26] of H^+ and Li^+, which would allow us to estimate a value of −410 ± 5 kcal/mol for the free energy of solvation of UO_2^{2+}. However, in our previous work, we were able to demonstrate convergence by calculations on larger clusters. We were unable to converge the wave functions with the SCIPCM for larger clusters with more than one solvation shell to demonstrate this convergence. Our values do not support the higher range of values near −470 kcal/mol reported by Cao and Balasubramanian[44] based on cluster/continuum models but are consistent with their values near −421 kcal/mol reported for the naked uranyl ion. Our results are consistent with the experimental values[40] and those calculated at the quasichemical level[21a] for the hydration free energies of divalent metal cations (M^{2+}), which largely fall in the range (with a few exceptions, such as Ca^{2+} and Be^{2+}) −390 to −480 kcal/mol. The hydration free energy of UO_2^{2+} is comparable to early first row transition metals ions, such as Sc^{2+}, Ti^{2+}, V^{2+}, Cr^{2+}, and Mn^{2+}, which fall on the more positive range of values, due to the relatively larger ionic radii.

Conclusions

Previous computational studies on actinide-containing complexes have indicated the importance of including solvation effects to obtain accurate geometries and relative energies of various species in solution based on using polarizable continuum models (PCM) with clusters. We have shown that the use of PCM models to study the change in free energy of the water exchange reaction for the addition of a single water molecule to $UO_2(H_2O)_4^{2+}$ has many difficulties. Successful use of PCM models requires that the parameters be properly chosen as the

results vary greatly with surface type, cavity size, and continuum method. We have shown that the contribution of the free energy of solvation to the reaction free energy is sensitive to modest changes in the oxygen and hydrogen radii, although the method is less sensitive to the choice of the uranium radius as this atom is buried in the center of the cluster. We have shown that the PCM model can successfully predict the free energy of the exchange reaction in aqueous solution, although the experimental free energy (−1.2 kcal/mol favoring the pentaaquo species) from the HEXS experiment was necessary to benchmark variations in the reaction field parameters. Although the SCIPCM approach avoids the use of atomic radii, it does require an isocontour level for the electron density that is inside the cavity. We found that the free energy of solvation was very sensitive to this value in the region where good agreement is found for the thermodynamics of reaction 1 and was larger than the value of 0.001 au recommended for neutral species.[79] The PCM models can successfully be used in computational studies of the thermodynamics of exchange reactions involving actinyl dication complexes but care must be taken in the choice of the parameters.

Inclusion of explicit water molecules in the second hydration sphere coupled with the PCM solvation model to treat the remaining solvent resulted in very good agreement with experiment in most cases. The rearrangement reactions from reactions 6 and 7 gave the best results, and there is no need to account for free water particles in the reaction energetics. Reactions 6 and 7 give deviations from experiment by +3.3 and +3.0 kcal/mol, respectively using the gas-phase MP2 energies and suggest that the four-coordinate structure is favored. When a PCM model with nonelectrostatic effects is included, both reactions 6 and 7 are predicted to favor the five-coordinate structure in agreement with experiment and are too negative by 1.3 and 0.9 kcal/mol, respectvely. Thus nearly all of the solvation effects for reaction 1 can be accounted for by inclusion of a second solvent shell around the waters directly bonded to the uranyl. Much of the reaction free energy can be rationalized on the basis of electronic effects only, based largely on a destabilization of the pentaaquo ion by the second hydration sphere and charge-transfer effects. Reactions 3−5 also gave excellent agreement with experiment in which water monomer, dimer, and trimer particles were used, indicating that good results can be obtained in these cases with a proper entropic treatment of the free particles is made. However, the use of rearrangement reactions is more desirable to avoid this problem.

The free energy of solvation of the uranyl cation is successfully modeled using both individual water molecules and water clusters at the SCIPCM level for 4 and 5 waters, and with water clusters (12 and 15 waters) at the PCM level. At the SCIPCM level, the average free energy of solvation was -410 ± 5 kcal/mol, which agreed well with the average free energy at the PCM level of -410 ± 2 kcal/mol. Overall, the upper bound to the uranyl solvation energy was established to be about -410 ± 4 kcal/mol including both the PCM and SCIPCM results. These results are consistent with those of Shamov and Schreckenbach[48] who proposed a value of −413.5 kcal/mol, as well as the best experimental value of -421 ± 15 kcal/mol. The free energy seems to be reasonably well converged using only a single hydration sphere, and inclusion of water molecules in the second sphere does not appear to substantially improve the free energy of solvation. Our results show that previously reported free energy values at -322 ± 5 kcal/mol and near −470 kcal/mol are likely too high and too low, respectively.

Acknowledgment. We thank Dr. L. Soderholm for bringing this problem to our attention and for sharing results with us. This research was supported in part by the U.S. Department of Energy, Environmental Management Sciences Program (EMSP) of the Department of Energy under a project entitled "A New Class of Solvents for TRU Dissolution and Separation: Ionic Liquids", Project No. 94640. This work was supported in part by the U.S. Department of Energy, Office of Basic Energy Sciences, Geosciences Research Program. D.A.D. is indebted to the Robert Ramsay Endowment of the University of Alabama. This research was performed in part using the Molecular Science Computing Facility (MSCF) in the William R. Wiley Environmental Molecular Sciences Laboratory, a national scientific user facility sponsored by the U.S. Department of Energy's Office of Biological and Environmental Research and located at the Pacific Northwest National Laboratory operated for the Department of Energy by Battelle.

Supporting Information Available: Radii, volumes, and energetic data for explicit radii. Molecular *x*, *y*, *z* coordinates of the optimized structures. This material is available free of charge via the Internet at http://pubs.acs.org.

References and Notes

(1) (a) Rizkalla, E. N.; Choppin, G. R. In *Handbook on the Physics and Chemistry of Rare Earths*; Gschneidner, K. A., Jr., Eyring, L., Choppin, G. R., Lander, G. H., Eds.; Lanthanides/Actinides: Chemistry; North-Holland: New York, 1994; Vol. 18, pp 529−558. (b) Choppin, G. R.; Rizkalla, E. N. In *Handbook on the Physics and Chemistry of Rare Earths*; Gschneidner, K. A., Jr., Eyring, L., Choppin, G. R., Lander, G. H., Eds.; Lanthanides/Actinides: Chemistry; North-Holland: New York, 1994; Vol. 18, pp 559−590. (c) Choppin, G. R. *J. Less-Common Met.* **1983**, *93*, 323−330. (d) Choppin, G. R.; Wong, P. J. *Aquatic Geochem.* **1998**, *4*, 77−101. (e) Nash, K. L. *Sep. Sci. Technol.* **1999**, *34*, 911−929.

(2) (a) Gutowski, K. E.; Bridges, N. J.; Rogers, R. D. In *Chemistry of the Actinide and Transactinide Elements*, 3rd ed.; Morss, L. R., Edelstein, N. M., Fuger, J., Katz, J. J., Eds.; Springer: Berlin (in press). (b) Burns, P. C.; Ewing, R. C.; Hawthorne, F. C. *Can. Miner.* **1997**, *35*, 1551−1570.

(3) (a) Sullens, T. A.; Jensen, R. A.; Shvareva, T. Y.; Albrecht-Schmitt, T. E. *J. Am. Chem. Soc.* **2004**, *126*, 2676−2677. (b) Sarsfield, M. J.; Helliwell, M. *J. Am. Chem. Soc.* **2004**, *126*, 1036−1037.

(4) (a) Fanghänel, T.; Neck, V. *Pure Appl. Chem.* **2002**, *74*, 1895−1970. (b) Clark, D. L.; Hobart, D. E.; Neu, M. P. *Chem. Rev.* **1995**, *95*, 25−48. (c) Casellato, U.; Vigato, P. A.; Vidali, M. *J. Coord. Chem.* **1981**, *36*, 183−265. (d) Neuefeind, J.; Skanthakumar, S.; Soderholm, L. *Inorg. Chem.* **2004**, *43*, 2422−2426. (e) Locock, A. J.; Burns, P. C. *J. Solid State Chem.* **2002**, *163*, 275−280. (f) Casellato, U.; Vigato, P. A.; Vidali, M. *Coord. Chem. Rev.* **1978**, *26*, 85−159. (g) Clark, D. L.; Keogh, D. W.; Palmer, P. D.; Scott, B. L.; Tait, C. D. *Angew. Chem., Int. Ed. Engl.* **1998**, *37*, 164−5. (h) Thuéry, P.; Nierlich, M.; Harrowfield, J. M.; Ogden, M. I. In *Calixarenes 2001*; Asfari, Z., Böhmer, V., Harrowfield, J., Vicens, J., Eds.; Kluwer Academic: Dordrecht, 2001; pp 561−582.

(5) (a) Alexander, V. *Chem. Rev.* **1995**, *95*, 273−342. (b) Sessler, J. L.; Seidel, D.; Vivian, A. E.; Lynch, V.; Scott, B. L.; Keogh, D. W. *Angew. Chem., Int. Ed. Engl.*, **2001**, *40*, 591−594. (c) Wrobleski, D. A.; Cromer, D. T.; Ortiz, J. V.; Rauschfuss, T. B.; Ryan, R. R.; Sattelberger, A. P. *J. Am. Chem. Soc.* **1986**, *108*, 174−175. (d) Evans, W. J.; Kozimor, S. A.; Ziller, J. W. *Science* **2005**, *309*, 1835−1838. (e) Crawford, M. J.; Ellern, A.; Mayer, P. *Angew. Chem., Int. Ed.* **2005**, *44*, 7874−7878. (f) Taylor, J. C. *Coord. Chem. Rev.* **1976**, *20*, 197−273.

(6) Hemmingsen, L.; Amara, P.; Ansoborlo, E.; Field, M. J. *J. Phys. Chem. A* **2000**, *104*, 4095−4101.

(7) Clavaguéra-Sarrio, C.; Brenner, V.; Hoyau, S.; Marsden, C. J.; Millié, P.; Dognon, J.-P. *J. Phys. Chem. B* **2003**, *107*, 3051−3060.

(8) (a) Sémon, L.; Boehme, C.; Billard, I.; Hennig, C.; Lützenkirchen, K.; Reich, T.; Rossberg, A.; Rossini, I.; Wipff, G. *Chem. Phys. Chem.* **2001**, *2*, 591−598. (b) Wahlgren, U.; Moll, H.; Grenthe, I.; Schimmelpfennig, B.; Maron, L.; Vallet, V.; Gropen, O. *J. Phys. Chem. A* **1999**, *103*, 8257−8264.

(9) Campbell, L.; Rehr, J. J.; Schenter, G. K.; McCarthy, M. I.; Dixon, D. A. *J. Synchroton Rad.* **1999**, *6*, 310−312.

(10) (a) Farkas, I.; Bányai, I.; Szabó, Z.; Wahlgen, U.; Grenthe, I. *Inorg. Chem.* **2000**, *39*, 799−805. (b) Vallet, V.; Wahlgren, U.; Schimmelpfennig, B.; Szabó, Z.; Grenthe, I. *J. Am. Chem. Soc.* **2001**, *123*, 11999−12008. (c) Vallet, V.; Privalov, T.; Wahlgren, U.; Grenthe, I. *J. Am. Chem. Soc.* **2004**, *126*, 7766−7767.

(11) (a) Toth, L. M.; Begun, G. M. *J. Phys. Chem.* **1981**, *85*, 547−549. (b) Basile, L. J.; Sullivan, J. C.; Ferraro J. R.; LaBonville, P. *Appl. Spectrosc.* **1974**, *28*, 142−145. (c) Jones, L. H.; Penneman, R. A. *J. Chem. Phys.* **1952**, *21*, 542−544. (d) Quilès, F.; Burneau, A. *Vibr. Spectrosc.* **2000**, *23*, 231−241.

(12) Åberg, M.; Ferri, D.; Glaser, J.; Grenthe, I. *Inorg. Chem.* **1983**, *22*, 3986−3989.

(13) Bardin, N.; Rubini, P.; Madic, C. *Radiochim. Acta* **1998**, *83*, 189−194.

(14) Alcock, N. W.; Esperas, S. J. *J. Chem. Soc., Dalton Trans.* **1977**, 893−896.

(15) Fischer, A. *Z. Anorg. Allg. Chem.* **2003**, *629*, 1012−1016.

(16) Deshayes, L.; Keller, N.; Lance, M.; Nierlich, M.; Vigner, J.-D. *Acta Crystallogr., Sect. C* **1994**, *50*, 1541−1544.

(17) Allen, P. G.; Bucher, J. J.; Shuh, D. K.; Edelstein, N. M.; Reich, T. *Inorg. Chem.* **1997**, *36*, 4676−4683.

(18) (a) Neuefeind, J.; Soderholm, L.; Skanthakumar, S. *J. Phys. Chem. A* **2004**, *109*, 2733−2739. (b) Soderholm, L.; Skanthakumar, S.; Neuefeind, J. *Anal. Bioanal. Chem.* **2005**, *383*, 48−55.

(19) (a) Kaltsoyannis, N. *Chem. Soc. Rev.* **2003**, *32*, 9−16. (b) de Jong, W. A.; Aprà, E.; Windus, T. L.; Nichols, J. A.; Harrison, R. J.; Gutowski, K. E.; Dixon, D. A. *J. Phys. Chem. A* **2005**, *109*, 11568−11577. (c) Schreckenbach, G.; Hay, J. P.; Martin, R. L. *J. Comput. Chem.* **1999**, *20*, 70−90. (d) Hay, P. J.; Martin, M. L. *Los Alamos Sci.* **2000**, *26*, 382−391.

(20) Tomasi, J.; Mennucci, B.; Cammi, R. *Chem. Rev.* **2005**, *105*, 2999−3094.

(21) (a) Asthagiri, D.; Pratt, L. R.; Paulaitis, M. E.; Rempe, S. B. *J. Am. Chem. Soc.* **2004**, *126*, 1285−1289. (b) Westphal, E.; Pliego, J. R., Jr. *J. Chem. Phys.* **2005**, *123*, 074508-1-07508-7.

(22) (a) Pavlov, M.; Siegbahn, P. E. M.; Sandström, M. *J. Phys. Chem. A* **1998**, *102*, 219−228. (b) Marcos, E. S.; Pappalardo, R. R.; Rinaldi, D. *J. Phys. Chem.* **1991**, *95*, 8928−8932. (c) Asthagiri, D.; Pratt, L. R. *Chem. Phys. Lett.* **2003**, *371*, 613−619. (d) Katz, A. K.; Glusker, J. P.; Beebe, S. A.; Bock, C. W. *J. Am. Chem. Soc.* **1996**, *118*, 5752−5763.

(23) Martínez, J. M.; Pappalardo, R. R.; Marcos, E. S. *J. Phys. Chem. A* **1997**, *101*, 4444−4448.

(24) Cosentino, U.; Villa, A.; Pitea, D.; Moro, G.; Barone, V. *J. Phys. Chem. B* **2000**, *104*, 8001−8007.

(25) Asthagiri, D.; Pratt, L. R.; Ashbaugh, H. S. *J. Chem. Phys.* **2003**, *119*, 2702−2708.

(26) (a) Zhan, C.-G.; Dixon, D. A. *J. Phys. Chem. A* **2001**, *105*, 11534−11540. (b) Zhan, C.-G.; Dixon, D. A. *J. Phys. Chem. A* **2002**, *106*, 9737−9744. (c) Zhan, C.-G.; Dixon, D. A. *J. Phys. Chem. B* **2003**, *107*, 4403−4417. (d) Zhan, C.-G.; Dixon, D. A. *J. Phys. Chem. A* **2004**, *108*, 2020−2029.

(27) Rotzinger, F. P. *Helv. Chim. Acta* **2000**, *83*, 3006−3020.

(28) Spencer, S.; Gagliardi, L.; Handy, N. C.; Ioannou, A. G.; Skylaris, C.-K.; Willetts, A.; Simper, A. M. *J. Phys. Chem. A* **1999**, *103*, 1831−1837.

(29) Hay, P. J. *J. Chem. Phys.* **1983**, *79*, 5469−5482.

(30) Martinez, J. M.; Pappalardo, R. R.; Marcos, E. S.; Mennucci, B.; Tomasi, J. *J. Phys. Chem. B* **2002**, *106*, 1118−1123.

(31) Hay, P. J.; Martin, R. L.; Schreckenbach, G. *J. Phys. Chem. A* **2000**, *104*, 6259−6270.

(32) Hay, P. J.; Martin, R. L. *J. Chem. Phys.* **1998**, *109*, 3875−3881.

(33) Tsushima, S.; Suzuki, A. *J. Mol. Struct. (THEOCHEM)* **2000**, *529*, 21−25.

(34) Ortiz, J. V.; Hay, R. L.; Martin, J. *J. Am. Chem. Soc.* **1992**, *114*, 2736−2737.

(35) Tsushima, S.; Yang, T.; Suzuki, A. *Chem. Phys. Lett.* **2001**, *334*, 365−373.

(36) Fuchs, M. S. K.; Shor, A. M. Rösch, N. *Int. J. Quantum Chem.* **2002**, *86*, 487−501.

(37) Minami, T.; Matsuoka, O. *Theo. Chim. Acta* **1995**, *90*, 27−39.

(38) Poirer, R.; Kari, R.; Csizmadia, I. G. *Handbook of Gaussian Basis Sets*; Elsevier: Amsterdam, 1985.

(39) Cornehl, H. H.; Heinemann, C.; Marçalo, J.; Pires de Matos, A.; Schwarz, H. *Angew. Chem., Int. Ed. Engl.* **1996**, *35*, 891−894.

(40) Marcus, Y. *Ion Solvation*; John Wiley & Sons Ltd.: New York, 1985; p 107.

(41) Hagberg, D.; Karlström, G.; Roos, B. O.; Gagliardi, L. *J. Am. Chem. Soc.* **2005**, *127*, 14250−14256.

(42) Bühl, M.; Diss, R.; Wipff, G. *J. Am. Chem. Soc.* **2005**, *127*, 13506−13507.

(43) Moskaleva, L. V.; Kruger, S.; Spörl, A.; Rösch, N. *Inorg. Chem.* **2004**, *43*, 4080−4090.

(44) Cao, Z.; Balasubramanian, K. *J. Chem. Phys.* **2005**, *123*, 114309−114321.

(45) Ermler, W. C.; Ross, R. B.; Christiansen, P. A. *Int. J. Quanum Chem.* **1991**, *40*, 829−846.

(46) Pacios, L. F.; Christiansen, P. A. *J. Chem. Phys.* **1985**, *82*, 2664−2671.

(47) Van Duijneveldt, F. B. IBM Technol. Res. Report No. RF1971, 945.

(48) Shamov, G. A.; Schreckenbach, G. *J. Phys. Chem. A* **2005**, 10961−10974.

(49) Küchle, W.; Dolg, M.; Stoll, H.; Preuss, H. *J Chem. Phys.* **1994**, *100*, 7535−7542.

(50) Marcus, Y. *J. Inorg. Nucl. Chem.* **1975**, *47*, 493−501.

(51) Gibson, H. K.; Haire, R. G.; Santos, G.; Marcalo, J.; Pires de Matos, A. *J. Phys. Chem. A* **2005**, *109*, 2768−2781.

(52) Becke, A. D. *J. Chem. Phys.* **1993**, *98*, 5648−5652. Lee, C.; Yang, W.; Parr, R. G. *Phys. Rev. B* **1988**, *37*, 785−789.

(53) Vosko, S. H.; Wilk, L.; Nusair, M. *Can. J. Chem.* **1980**, *58*, 1200−1211. Slater, J. C. *Phys. Rev.* **1951**, *81*, 385−390. We used the SVWN5 version as implemented in Gaussian-03.

(54) Cao, X.; Dolg, M.; Stoll, H. *J. Chem. Phys.* **2003**, *118*, 487−496.

(55) Godbout, N.; Salahub, D. R.; Andzelm, J.; Wimmer, E. *Can. J. Chem.* **1992**, *70*, 560−571.

(56) Dunning, T. H., Jr. *J. Chem. Phys.* **1989**, *90*, 1007−1023.

(57) Fine grids (Krack, M.; Koster, A. M. *J. Chem. Phys.* **1998**, *108*, 3226−3234) were used in the DFT calculations. No changes in geometries and vibrations was observed with ultrafine grids.

(58) Privalov, T.; Schimmelpfennig, B.; Wahlgren, U.; Grenthe, I. *J. Phys. Chem. A* **2002**, *106*, 11277−11282.

(59) Frisch, M. J.; Trucks, G. W.; Schlegel, H. B.; Scuseria, G. E.; Robb, M. A.; Cheeseman, J. R.; Montgomery, J. A., Jr.; Vreven, T.; Kudin, K. N.; Burant, J. C.; Millam, J. M.; Iyengar, S. S.; Tomasi, J.; Barone, V.; Mennucci, B.; Cossi, M.; Scalmani, G.; Rega, N.; Petersson, G. A.; Nakatsuji, H.; Hada, M.; Ehara, M.; Toyota, K.; Fukuda, R.; Hasegawa, J.; Ishida, M.; Nakajima, T.; Honda, Y.; Kitao, O.; Nakai, H.; Klene, M.; Li, X.; Knox, J. E.; Hratchian, H. P.; Cross, J. B.; Bakken, V.; Adamo, C.; Jaramillo, J.; Gomperts, R.; Stratmann, R. E.; Yazyev, O.; Austin, A. J.; Cammi, R.; Pomelli, C.; Ochterski, J. W.; Ayala, P. Y.; Morokuma, K.; Voth, G. A.; Salvador, P.; Dannenberg, J. J.; Zakrzewski, V. G.; Dapprich, S.; Daniels, A. D.; Strain, M. C.; Farkas, O.; Malick, D. K.; Rabuck, A. D.; Raghavachari, K.; Foresman, J. B.; Ortiz, J. V.; Cui, Q.; Baboul, A. G.; Clifford, S.; Cioslowski, J.; Stefanov, B. B.; Liu, G.; Liashenko, A.; Piskorz, P.; Komaromi, I.; Martin, R. L.; Fox, D. J.; Keith, T.; Al-Laham, M. A.; Peng, C. Y.; Nanayakkara, A.; Challacombe, M.; Gill, P. M. W.; Johnson, B.; Chen, W.; Wong, M. W.; Gonzalez, C.; Pople, J. A. *Gaussian 03*, revision B.05; Gaussian, Inc.: Wallingford, CT, 2004.

(60) Aprà, E.; Windus, T. L.; Straatsma, T. P.; Bylaska, E. J.; de Jong, W.; Hirata, S.; Valiev, M.; Hackler, M.; Pollack, L.; Kowalski, K.; Harrison, R.; Dupuis, M.; Smith, D. M. A.; Nieplocha, J.; Tipparaju V.; Krishnan, M.; Auer, A. A.; Brown, E.; Cisneros, G.; Fann, G.; Fruchtl, H.; Garza, J.; Hirao, K.; Kendall, R.; Nichols, J.; Tsemekhman, K.; Wolinski, K.; Anchell, J.; Bernholdt, D.; Borowski, P.; Clark, T.; Clerc, D.; Dachsel, H.; Deegan, M.; Dyall, K.; Elwood, D.; Glendening, E.; Gutowski, M.; Hess, A.; Jaffe, J.; Johnson, B.; Ju, J.; Kobayashi, R.; Kutteh, R.; Lin, Z.; Littlefield, R.; Long, X.; Meng, B.; Nakajima, T.; Niu, S.; Rosing, M.; Sandrone, G.; Stave, M.; Taylor, H.; Thomas, G.; van Lenthe, J.; Wong, A.; Zhang, Z. NWChem, A Computational Chemistry Package for Parallel Computers, Version 4.7; Pacific Northwest National Laboratory: Richland, WA 99352-0999, 2005. Kendall, R. A.; Apra, E.; Bernholdt, D. E.; Bylaska, E. J.; Dupuis, M.; Fann, G. I.; Harrison, R. J.; Ju, J.; Nichols, J. A.; Nieplocha, J.; Straatsma, T. P.; Windus, T. L.; Wong, A. T. *Comput. Phys. Commun.* **2000**, *128*, 260−283.

(61) Miertš, S.; Scrocco, E.; Tomasi, *J. Chem. Phys.* **1981**, *55*, 117−129.

(62) Barone, V.; Cossi, M. *J. Phys. Chem A* **1998**, *102*, 1995−2001.

(63) Foresman, J. B.; Keith, T. A.; Wiberg, K. B.; Snoonian, J.; Frisch, M. J. *J. Phys. Chem.* **1996**, *100*, 16098−16104.

(64) Klamt, A.; Schüürmann, G. *J. Chem. Soc., Perkin Trans. 2* **1993**, 799−805.

(65) (a) Rappe, A. K.; Casewit, C. J.; Colwell, K. S.; Goddard, W. A.; Skiff, W. M. *J. Am. Chem. Soc.* **1992**, *114*, 10024−10035. (b) Barone, V.; Cossi, M.; Tomasi, J. *J. Chem. Phys.* **1997**, *107*, 3210−3221. (c) Pauling, L. *The Nature of the Chemical Bond*, 3rd ed.; Cornell University Press: Ithaca, NY, 1960. (d) Bondi, A. *J. Phys. Chem.* **1964**, *68*, 441−451.

(66) (a) Reed, A. E.; Curtiss, L. A.; Weinhold, F. *Chem. Rev.* **1988**, *88*, 899−926. (b) Foster, J. P.; Weinhold, F. *J. Am. Chem. Soc.* **1980**, *102*, 7211−7218. (c) Reed, A. E.; Weinhold, F. *J. Chem. Phys.* **1983**, *78*, 4066−4073. (d) Reed, A. E.; Weinstock, R. B.; Weinhold, F. *J. Chem. Phys.* **1985**, *83*, 735−746. (e) Reed, A. E.; Weinhold, F. *J. Chem. Phys.* **1985**, *83*, 1736−1740.

(67) Johnson, B. G.; Gill, P. M. W.; Pople, J. A. *J. Chem. Phys.* **1993**, *98*, 5612−5626.

(68) García-Hernández, M.; Lauterbach, C.; Krüger, S.; Matveev, A.; Rösch, N. *J. Comput. Chem.* **2002**, *23*, 834−846.

(69) Lee, T. J.; Rice, J. E.; Scuseria, G. E.; Schaefer, H. F., III. *Theor. Chim. Acta* **1989**, *75*, 81−98.

(70) Takanao, Y.; Houk, K. N. T. *J. Chem. Theory Comput.* **2005**, *1*, 70−77.

(71) Curutchet, C.; Bidon-Chanal, A.; Soteras, I.; Orozco, M.; Luque, F. J. *J. Phys. Chem. B* **2005**, *109*, 3565−3574.

(72) SCIPCM electrostatic contributions were done with respect to the gas-phase B3LYP/TZVP/Stuttgart energies for the three species. Also, an isodensity value of 0.001 for water was used for all energetics.

(73) (a) Dixon, D. A.; Feller, D.; Zhan, C.-G.; Francisco, J. S. *Int. J. Mass Spectrom.* **2003**, *227*, 421−438. (b) Alexeev, Y.; Windus, T. L.; Dixon, D. A.; Zhan, C.-G. *Int. J. Quantum Chem.* **2005**, *102*, 775−784; **200**5, *104*, 379−380 (erratum).

(74) (a) Ben-Naim, A.; Marcus, Y. *J. Chem. Phys.* **1984**, *81*, 2016−2027. (b) Marcus, Y. *Biophys. Chem.* **1994**, *51*, 111−127. (c) Hummer, G.; Pratt, L. R.; García, A. E. *J. Phys. Chem.* **1996**, *100*, 1206−1215. (d) Martin, R. L.; Hay, P. .J.; Pratt, L. R. *J. Phys. Chem. A* **1998**, *102*, 3565−3573.

(75) Optimization of the uranyl aquo ions using SCIPCM met with substantial difficulties, particularly with respect to obtaining the frequencies. Imaginary frequencies were prevalent and difficult to eliminate, and thus structural details were not reported, although they are consistent with the cluster values in the case of $UO_2(H_2O)_5^{2+}$.

(76) (a) Dang, L. X. *J. Phys. Chem. B* **1998**, *102*, 620−624. (b) Dang, L. X.; Chang, T.-M. *J. Chem. Phys.* **1997**, *106*, 8149−8159. (c) Dang, L. X.; Rice, J. E.; Caldwell, J.; Kollman, P. A. *J. Am. Chem. Soc.* **1991**, *113*, 2481−2486.

(77) Feyereisen, M. W.; Feller, D.; Dixon, D. A. *J. Phys. Chem.* **1996**, *100*, 2993−2997.

(78) The pressure correction for the $(H_2O)_n$ clusters is calculated as $-4.3/n$.

(79) (a) Zhan, C.-G.; Bentley, J.; Chipman, D. M. *J. Chem. Phys.* **1998**, *108*, 177−192. (b) Zhan, C.-G.; Chipman, D. M. *J. Chem. Phys.* **1998**, *109*, 10543−10558. (c) Zhan, C.-G.; Chipman, D. M. *J. Chem. Phys.* **1999**, *110*, 1611−1622. (d) Zhan, C.-G.; Landry, D. W.; Ornstein, R. L. *J. Phys. Chem. A* **2000**, *104*, 7672−7678.